FINAL REPORT
DEVELOPMENT OF A BAGASSE PELLETING MACHINE USING A ROLLING PRINCIPLE

PART B
UNIVERSITY OF QUEENSLAND COMPONENT

A23187573B

PROJECT TITLE:	DEVELOPMENT OF A BAGASSE PELLETING MACHINE USING A ROLLING PRINCIPLE, 82/2435.
DATE OF ISSUE:	1982
AUTHORS:	PART A. SUGAR RESEARCH INSTITUTE R. CULLEN V. MASON PART B. UNIVERSITY OF QUEENSLAND R. CULLEN R. STALKER P. KILLEN
NAMES OF ORGANISATIONS:	SUGAR RESEARCH INSTITUTE AND DEPARTMENT OF MECHANICAL ENGINEERING, UNIVERSITY OF QUEENSLAND.
TOTAL EXPENDITURE UNDER GRANT:	$93 960

DEVELOPMENT OF A BAGASSE PELLETING MACHINE USING A ROLLING PRINCIPLE

CONTENTS

DEVELOPMENT OF A BAGASSE PELLETING MACHINE USING A ROLLING PRINCIPLE 82/2435

SUMMARY

The project report consists of two parts. The University of Queensland component describes the results of tests to establish information on basic properties of bagasse that are of significance in the design of a rolling pelleting machine. These properties include the dynamic compression and relaxation characteristics under normal and sinusoidal (as developed in a rolling pelleter) compression, the frictional properties, and the energy required to compact the bagasse. The properties were measured over a range of variables such as temperature, moisture content and particle size.

The properties of single fibres were investigated and a theory has been proposed to explain the compaction process.

The Sugar Research Institute component of the report describes the development of the rolling pelleting machine. The pilot plant machine was able to produce pellets of up to the design density of 500 kg/m^3 at a rate of up to 500 kg/h. This throughput was below that originally predicted due to feeding problems with the light low moisture material. Difficulties were experienced with scraper action of the roll scrapers.

The pilot plant and trials established the feasibility of the rolling principle for pellet production. Further development is required before a 'production' unit can be produced.

PART B: UNIVERSITY OF QUEENSLAND COMPONENT

CHAPTER 1

INTRODUCTION

The objectives of the project have been outlined in Part A - the Sugar Research Institute component of the work. The investigations at the Department of Mechanical Engineering, carried out under the present grant, considered further the influence of precompression by rolling, retention, particle size, temperature and moisture on the properties of the pellets produced. This work was initiated under the Project Grant "Elimination of the Use of Fuel Oil for Steam Generation in the Sugar Industry".

The opportunity was taken to use the facilities at the CSIRO Division of Textile Industry, Geelong, to study three dimensional compression characteristics of bagasse over a range of compression and retention times. This work confirmed that reasonable pellets could be obtained at the lower levels of press times achieved.

Work undertaken under the previous NERDDC grant showed that retention, i.e. holding a load on the bagasse sample after compression, was a significant way in which pellet properties could be improved. In an attempt to obtain an understanding of retention it was decided to investigate the relaxation characteristic of bagasse under conditions of both linear compression and sinusoidal compression which simulted the compression experienced in a rolling machine. The relaxation characteristics were studied over a wide range of operating conditions which included moisture content, temperature, level of compaction, speed of compaction, and particle size. The extent of relaxation can have a significant influence on the design of a pelleting machine, particularly in relation to discharge conditions.

In any pelleting machine the energy of compaction of the material is an important design parameter. Tests were carried out over a range of temperatures, speeds of compaction, bagasse moistures, bagasse fineness and levels of compaction to investigate their influence on the compaction energy.

In any practical pelleting machine friction plays a very important role. Both the rolling die and reciprocating type of pelleting machines rely on friction to supply the back pressure necessary to achieve compaction. As outlined in Part A of the report friction plays an important role in the two roll pelleter since friction on the rolls provide the driving force to push the material through the machine and also contributes to the back pressure supplied by the chutes. A series of tests was therefore carried out to investigate the coefficient of friction over a range of bagasse moisture, particle size, temperatures and pressures for a range of surface conditions.

An investigation of the literature on pelleting and compaction established that no theory exists for pelleting of agricultural waste materials such as bagasse. An effective theory for pelleting is necessary if a full understanding of the process is to be obtained. An attempt was made to develop a theory of compaction and the results are outlined in this report. The theory explains the pelleting process but does not cover the influence of retention.

CHAPTER 2
RESULTS OF TESTS AT CSIRO DIVISION OF TEXTILE INDUSTRY

2·1 INTRODUCTION

The CSIRO Division of Textile Industry has for many years now conducted tests on compaction of wool. As an essential part of this programme they have developed several presses to compact the wool under an approximation to triaxial conditions. The largest of the presses is shown schematically in Figure 2.1 This unit produces compressed blocks with typical dimensions 200 x 150 x 40 mm. Typical pellets are shown in Figure 2.2.

2·2 OPERATION OF PRESS

The sample to be compressed - typically 1.5 kg - is loaded into a metal box where it can be heated in a closed atmosphere by hot air. This ensures that the initial moisture content is retained. The heated material is then dropped into a hopper with a moveable side which allows the sample to be presented to a ram to apply an initial precompression. This extent of compression is dictated by the initial charge mass since the ram compresses to a constant height. After this initial compression the second ram applies a preset pressure to the sample. After a controlled hold time at this pressure the wad is ejected into a 'cold frame' where it can be held at fixed dimensions for a predetermined time.

2·3 TEST RESULTS

The objective of the tests was to investigate the influence of pressing time and retention time (time held in a 'cold box' of constant dimensions) on the resulting properties of the pellets.

The results of the test series for a range of press times from 0.5 to 5 minutes and retention times from 1 to 320 minutes are shown in Figures 2.3 and 2.4. The lower limits of press time

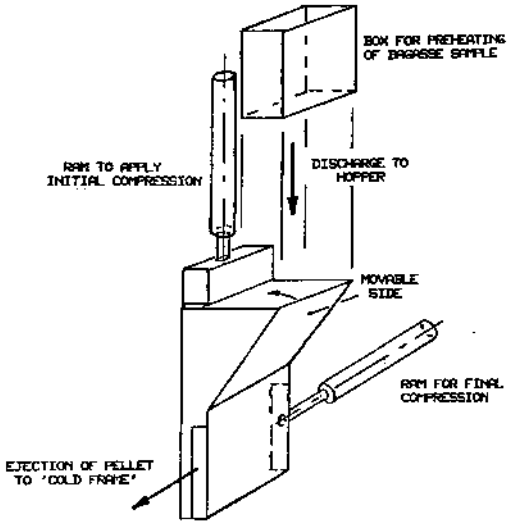

FIGURE 2.1 SCHEMATIC ARRANGEMENT OF PRESSING SYSTEM - CSIRO DIVISION OF TEXTILE INDUSTRY

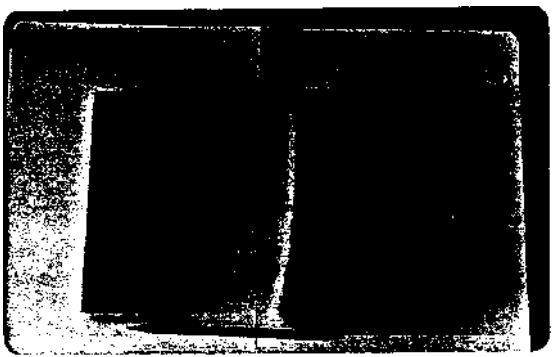

FIGURE 2.2 SAMPLE OF PELLET PRODUCED

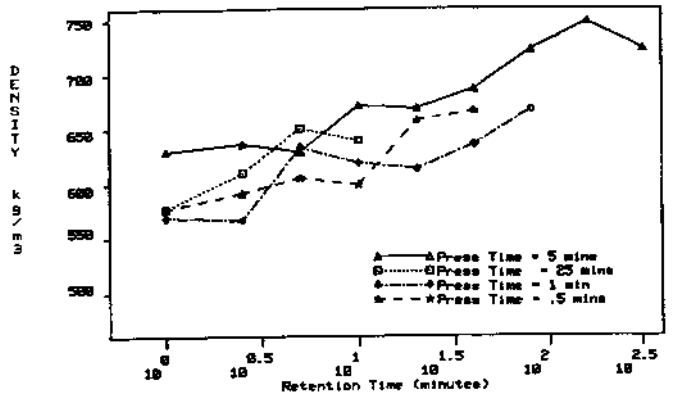

Conditions: Temperature 80° C; Moisture 8%; Material whole.

FIGURE 2·3 RELATIONSHIP BETWEEN DENSITY AT REMOVAL AND RETENTION TIME FOR A RANGE OF PRESS TIMES

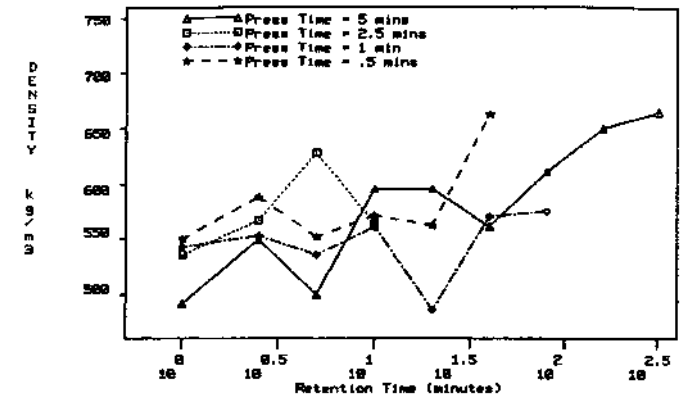

Conditions: Temperature 80° C; Moisture 8%; Material whole.

FIGURE 2·4 RELATIONSHIP BETWEEN DENSITY AFTER 12 HOURS AND RETENTION TIME FOR A RANGE OF PRESS TIMES

and retention time were dictated by the physical constraints of the machine.

The results illustrate that whilst increases in press time and retention increased the density of the pellet at removal, the densities after 12 hours were not adversely affected by reduction in press time at retention times down to the lower limit achievable in the test rig (1 minute). These results gave some confidence that the pressure and retention times planned for the rolling apparatus would produce acceptable pellet densities.

CHAPTER 3
TESTS WITH CRUCIFORM ROLLING MACHINE

3·1 INTRODUCTION

The cruciform rolling machine was developed under NERDDC grant 79/9389 'Elimination of Use of Fuel Oil for Steam Generation in the Sugar Industry'. Tests were carried out under that project over a range of temperatures, particle sizes, moisture contents and with and without precompression.

These tests were extended under the present NERDDC grant to investigate further the effects of higher temperature (140°). The tests were planned in a manner which enabled analysis of variance of the results to be carried out for the following 'block' of variables with replicates.

Precompression	C	Precompression; No Precompression.
Retention	X	No Retention; Retention.
Material	M	Total; Coarse; Medium; Fine.
Temperature	T	20°C; 80°C; 140°C.
Moisture	W	10%; 20%; 30%.

Tests were carried out at a pressure of 36 MPa and a dwell time of 8 seconds. Retention was for 2 minutes at 500 kPa.

The significant factors and interactions established in the analysis of variance are discussed below. The broader range of tests enables a more in depth review of results to be presented than that outlined in the final report of Project 79/9389.

Material specifications are as outlined in the report on Project 79/9389 (p 97):

"The fibre fractions were sieved from whole bagasse. About 30 shakes of the 250 mm diameter sieves of 2.8 mm and 0.6 mm aperture sizes gave three fibre definitions: coarse (< 2.8 mm), medium (< 2.8 mm, > 0.6 mm) and fine (< 0.6 mm). An additional fibre fraction consisted of the original whole bagasse. The fine fraction contained mostly small flaky pith particles with occasional tiny broken fibres. The medium fraction contained mostly thin fibres or vascular bundles with average length of about 10 mm. The coarse fraction necessarily contained the thick rind particles and long fibre bundles."

Full test results are shown in Tables 3.1 and 3.2. The results of the analysis of variance on the data are outlined in Tables 3.3 and 3.4.

3·2 SINGLE FACTOR EFFECTS

All variables, with the exception of precompression, had a significant effect on the density of the pellet at 24 hours. All variables had a significant effect on durability. The effect of the single variables, averaged over all other variables, is summarised below.

. PRECOMPRESSION

Figure 3.1 illustrates the fact that precompression had no significant effect on density at 24 hours but increased durability.

. RETENTION

Figure 3.2 illustrates the beneficial effect of retention to improve both density and durability.

. TEMPERATURE

Figure 3.3 shows that there is very little difference between densities obtained at 20° and 80°C but that densities at 140°C are inferior to those at 20° and 80°C. The durabilities show a similar trend.

TABLE 3.1 COMPACTIONS AT 24 h (kg/m^3 dry)

			T_1 = 20°C						T_2 = 80°C						T_3 = 140°C					
			W_1 = 10		W_2 = 20		W_3 = 30		W_1 = 10		W_2 = 20		W_3 = 30		W_1 = 10		W_2 = 20		W_3 = 30	
			R_1	R_2	R_1	R_2	R_1	R_2	R_1	R_2	R_1	R_2	R_1	R_2	R_1	R_2	R_1	R_2	R_1	R_2
No Precompression	Retention	M_1 Total	618	639	448	445	257	255	661	663	316	298	169	170	784	779	406	452	179	198
		M_2 Coarse	413	400	212	220	95	96	680	641	193	165	146	134	358	393	182	178	180	179
		M_3 Medium	531	510	386	180	134	122	675	710	225	233	130	146	413	391	210	235	115	116
		M_4 Fine	592	600	536	526	160	162	840	833	590	582	217	206	493	504	233	240	100	100
	No Retention	M_1 Total	535	522	375	350	239	256	487	408	174	188	139	143	567	619	358	359	197	-
		M_2 Coarse	319	303	194	200	106	99	431	422	114	136	144	140	295	307	140	118	125	140
		M_3 Medium	391	403	307	306	115	133	523	478	172	172	135	124	365	482	150	138	130	104
		M_4 Fine	485	475	388	391	143	145	543	518	442	408	142	130	486	556	261	187	116	100
Precompression	Retention	M_1 Total	658	647	435	456	229	218	745	691	325	314	189	217	856	854	436	405	183	217
		M_2 Coarse	444	455	277	221	107	111	611	622	212	231	136	134	510	544	188	166	134	146
		M_3 Medium	559	555	385	406	120	121	690	698	223	221	147	135	490	495	200	217	418	143
		M_4 Fine	547	546	513	514	159	164	750	808	273	334	162	175	472	562	235	291	162	-
	No Retention	M_1 Total	543	547	393	359	239	213	533	580	199	200	154	146	691	550	331	368	202	208
		M_2 Coarse	395	405	191	204	116	107	415	432	181	199	129	115	429	450	173	196	112	125
		M_3 Medium	457	437	310	241	124	119	515	523	205	172	147	148	346	497	151	141	115	110
		M_4 Fine	444	437	392	385	158	154	538	519	243	206	165	133	363	387	100	313	100	203

20°C - Old bagasse 1980 season

80°C - New bagasse 1982 season

TABLE 2.2 DURABILITY OF PELLETS (%)

				T_1 = 20°C						T_2 = 80°C						T_3 = 140°C					
				W_1 = 10		W_2 = 20		W_3 = 30		W_1 = 10		W_2 = 20		W_3 = 30		W_1 = 10		W_2 = 20		W_3 = 30	
				R_1	R_2	R_1	R_2	R_1	R_2	R_1	R_2	R_1	R_2	R_1	R_2	R_1	R_2	R_1	R_2	R_1	R_2
No Precompression C_1	Retention X_1	M_1	Total	94.5	95.4	94.9	94.0	74.5	4.4	98.2	98.5	93.4	92.0	79.0	76.0	99.0	98.4	96.4	97.3	19.7	12.0
		M_2	Coarse	57.5	44.9	20.9	42.5	-	-	98.3	96.4	53.2	57.3	4.1	9.2	93.1	90.7	28.5	39.0	31.6	38.7
		M_3	Medium	95.5	95.4	94.6	85.9	0.4	0.6	95.3	97.2	85.4	90.4	26.1	6.0	94.9	94.1	84.3	83.7	-	-
		M_4	Fine	93.5	92.5	94.8	94.6	81.7	79.9	96.7	96.5	96.8	97.2	94.5	90.8	99.4	95.4	94.6	90.8	-	-
	No Retention X_2	M_1	Total	89.9	88.9	88.4	88.9	63.0	2.0	94.8	90.0	76.2	54.0	42.0	49.0	97.5	98.0	93.5	91.7	35.2	6.6
		M_2	Coarse	30.2	27.2	1.5	5.2	-	-	88.7	75.6	3.0	6.1	1.1	-	79.5	71.7	6.0	4.0	12.2	22.8
		M_3	Medium	50.1	79.5	51.9	73.4	0.3	-	91.8	94.8	38.3	24.7	0.2	5.6	93.5	96.8	18.6	25.9	-	-
		M_4	Fine	70.0	65.3	78.7	79.1	74.2	54.5	80.4	91.8	92.6	88.5	76.7	76.4	94.7	96.2	76.5	73.3	35.2	53.9
Precompression C_2	Retention X_1	M_1	Total	97.6	97.6	94.5	95.5	50.1	9.6	98.5	98.9	96.9	96.3	96.0	90.0	99.3	98.9	98.4	97.4	22.9	64.4
		M_2	Coarse	91.0	88.5	82.3	40.8	0.7	-	99.7	99.6	92.0	93.0	18.0	18.0	99.1	99.6	66.2	65.0	41.8	50.9
		M_3	Medium	97.3	97.8	96.2	94.0	3.7	1.4	96.5	97.4	86.0	88.0	42.8	45.5	96.7	96.6	76.4	80.7	11.7	10.7
		M_4	Fine	92.1	93.9	95.0	94.8	81.9	79.3	94.0	96.7	92.4	96.7	84.4	86.2	96.4	98.5	87.9	92.5	-	-
	No Retention X_2	M_1	Total	96.3	92.8	90.1	90.4	59.3	6.4	95.3	97.6	73.2	67.0	75.0	68.0	98.1	98.9	92.9	97.4	57.6	27.1
		M_2	Coarse	82.1	84.1	40.9	52.2	0.7	-	89.6	98.6	62.0	89.0	12.0	-	99.2	99.2	69.8	58.1	11.1	29.1
		M_3	Medium	88.9	90.9	75.6	87.4	12.3	-	91.5	94.3	65.0	45.0	-	39.4	93.0	98.6	47.4	30.2	-	-
		M_4	Fine	82.3	67.5	81.4	83.2	79.6	74.8	86.3	84.8	86.1	78.8	71.6	70.8	87.1	91.5	82.3	75.8	-	58.3

TABLE 3.3 ANALYSIS OF VARIANCE RESULTS FOR DENSITY AT 24 H

Source	Degrees of Freedom	Variance Ratio	Significance Level
Total	287		
C	1	.084	
X	1	485.332	Less than .001
M	3	363.410	Less than .001
T	2	79.904	Less than .001
W	2	4933.458	Less than .001
CX	1	2.724	.100 - .250
CM	3	21.322	Less than .001
CT	2	3.117	.010 - .050
CW	2	5.113	.001 - .010
XM	3	4.813	.001 - .010
XT	2	42.466	Less than .001
XW	2	109.208	Less than .001
MT	6	68.440	Less than .001
MW	6	37.354	Less than .001
TW	4	131.836	Less than .001
CXM	3	2.060	.100 - .250
CXT	2	1.917	.100 - .250
CXW	2	.438	
CMT	6	10.819	Less than .001
CMW	6	8.665	Less than .001
CTW	4	2.725	.010 - .050
XMT	6	4.171	Less than .001
XMW	6	2.306	.010 - .350
XTW	4	19.735	Less than .001
MTW	12	10.885	Less than .001
CXMT	6	4.231	Less than .001
CXMW	6	3.118	.001 - .010
CXTW	4	.560	
CMTW	12	10.868	Less than .001
XMTW	12	1.240	Greater than .250
CXMTW	12	2.821	.001 - .010
ERROR	144		

TABLE 3.4 ANALYSIS OF VARIANCE RESULTS FOR DURABILITY

Source	Degrees of Freedom	Variance Ratio	Significance Level
Total	287		
C	1	56.515	Less than .001
X	1	93.166	Less than .001
M	3	157.395	Less than .001
T	2	26.062	Less than .001
W	2	769.978	Less than .001
CX	1	6.084	.010 - .050
CM	3	18.934	Less than .001
CT	2	.277	
CW	2	4.365	.010 - .050
XM	3	5.425	.001 - .010
XT	2	5.424	.001 - .010
Xw	2	14.156	Less than .001
MT	6	14.607	Less than .001
MW	6	34.468	Less than .001
TW	4	18.953	Less than .001
CXM	3	.964	
CXT	2	.923	
CXW	2	2.394	.050 - .100
CMT	6	1.213	Greater than .250
CMW	6	6.635	Less than .001
CTW	4	3.643	.001 - .010
XMT	6	2.197	.010 - .050
XMW	6	3.521	.001 - .010
XTW	4	3.438	.010 - .050
MTW	12	14.822	Less than .001
CXMT	6	.324	
CXMW	6	.792	
CXTW	4	.911	
CMTW	12	1.428	.100 - .250
XMTW	12	2.412	.001 - .010
CXMTW	12	.167	
ERROR	144		

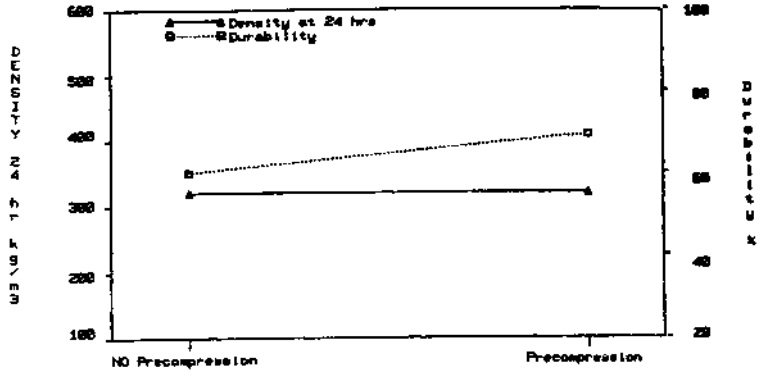

FIGURE 3·1 EFFECT OF PRECOMPRESSION ON DENSITY (AT 24 H) AND DURABILITY OF BAGASSE (RESULTS AVERAGED OVER OTHER VARIABLES)

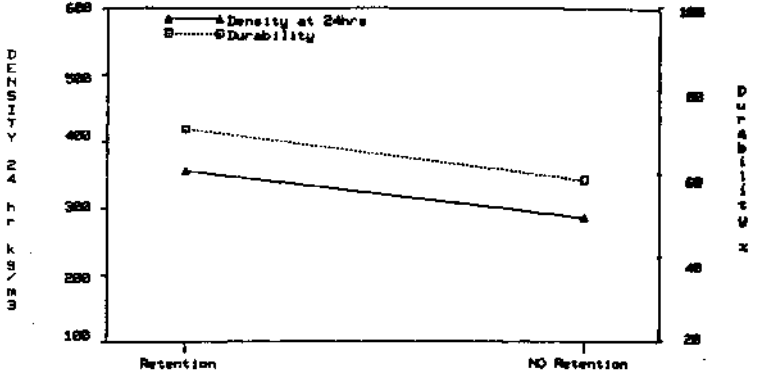

FIGURE 3·2 EFFECT OF RETENTION ON DENSITY (AT 24 H) AND DURABILITY OF BAGASSE (RESULTS AVERAGED OVER OTHER VARIABLES)

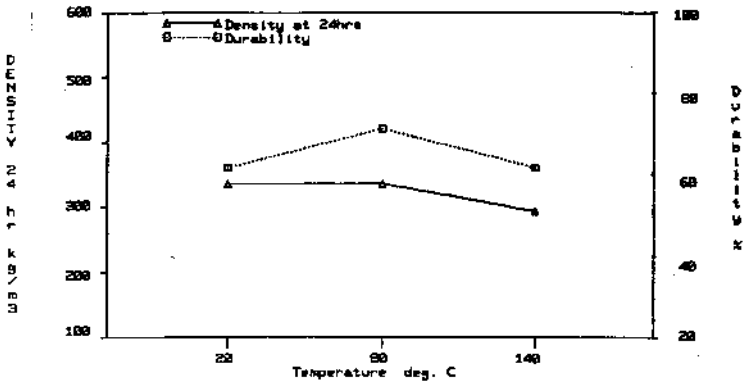

FIGURE 3.3 EFFECT OF TEMPERATURE ON DENSITY (AT 24 H) AND DURABILITY OF BAGASSE (RESULTS AVERAGED OVER OTHER VARIABLES)

. MOISTURE CONTENT
Figure 3.4 shows how densities and durabilities fall as moisture is increased in the range 10 to 30 per cent.

. PARTICLE SIZE
Figure 3.5 illustrates that the total material and fine material have similar pelleting characteristics and give better densities and durabilities than the coarse or medium fraction.

3·3 OTHER INTERACTIONS - DENSITY

In the following discussions only interactions that are of some practical significance will be discussed. They will be discussed in order of presentation in Table 3.3, i.e. any interaction between precompression and retention would be discussed under precompression.

3.3.1 INTERACTIONS INVOLVING PRECOMPRESSION

CM and CMW Interactions

Figure 3.6 illustrates the particle size, precompression interaction. This shows that there is a tendency for better performance with fine material when there is no precompression. Tests were carried out to determine the movement characteristics down the chute for the 2 : 1 compression system. These results, shown in Figure 3.7, show that whilst slippage occurs with 'whole', 'medium' and 'coarse', material could not be controlled for 'fine' material. Because of this lack of control with the fine material interactions which are explained by this phenomenon, e.g. CMT, will not be discussed further.

3.3.2 INTERACTIONS INVOLVING TEMPERATURE

Figure 3.8 illustrates the MT interaction which shows that pelleting densities are better for whole and worse for fine material than those obtained at 20° and 80° C.

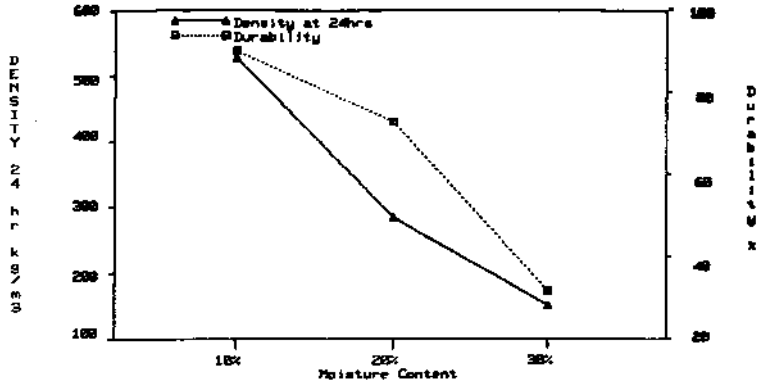

FIGURE 3·4 EFFECT OF MOISTURE CONTENT ON DENSITY (AT 24 H) AND DURABILITY OF BAGASSE (RESULTS AVERAGED OVER OTHER VARIABLES)

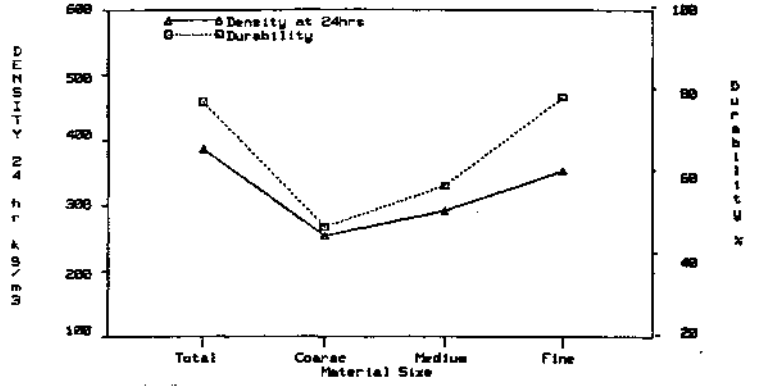

FIGURE 3·5 EFFECT OF MATERIAL SIZE ON DENSITY (AT 24 H) AND DURABILITY OF BAGASSE (RESULTS AVERAGED OVER OTHER VARIABLES)

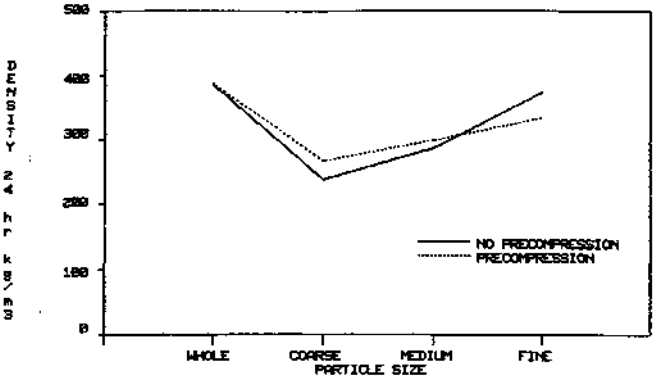

FIGURE 3·6 ILLUSTRATION OF PARTICLE SIZE-PRECOMPRESSION INTERACTION

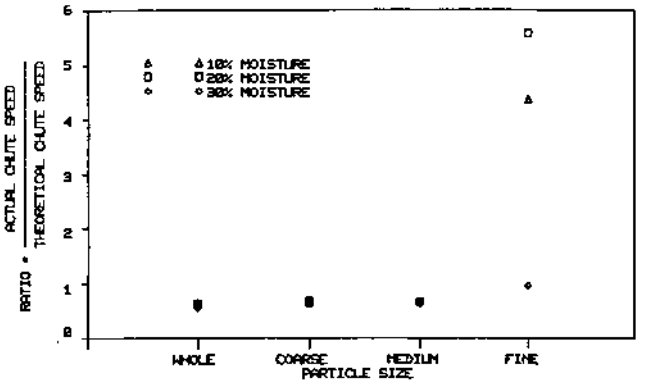

FIGURE 3·7 INFLUENCE OF PARTICLE SIZE AND MOISTURE CONTENT ON RATIO OF ACTUAL CHUTE SPEED TO THEORETICAL CHUTE SPEED

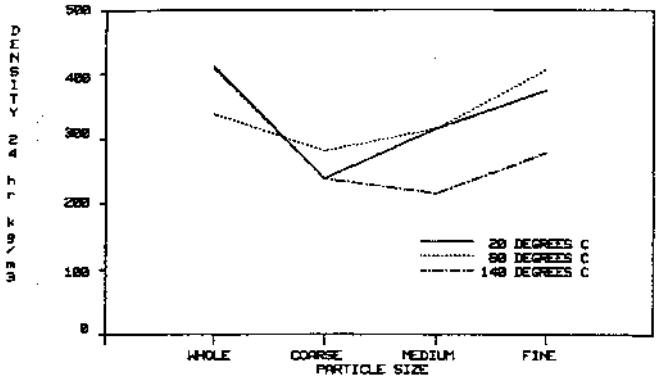

FIGURE 3·8 ILLUSTRATION OF PARTICLE SIZE AND TEMPERATURE INTERACTION

Figure 3.9 illustrates the XT interaction which shows that the effect of retention is enhanced at 80° compared with 20°C and 140°C.

The TW interaction is illustrated in Figure 3.10 and the XTW interaction is illustrated in Figure 3.11. The XTW interaction illustrates the fact that at 80°C the densities at 10 per cent moisture are better than those at 20° or 140°C whilst at 20 per cent moisture and 30 per cent moisture better results are obtained at 20°C. Best overall performance is at 80°C with retention. The relatively poor result for 140°C at 10 per cent moisture is surprising.

The most interesting aspect of this interaction is that the best compactions are obtained at 80° C and 10 per cent moisture. It is to be noted that the fall off in compaction with increase in moisture is more pronounced at higher temperatures.

3.3.3 INTERACTIONS INVOLVING MOISTURE

The XW interaction illustrated in Figure 3.12 illustrates the fact that the effect of precompression in increasing pellet density is more pronounced at lower moistures.

Figure 3.13 illustrates that response by 10 per cent and 20 per cent material is consistent one with the other for the different particle sizes but at 30 per cent moisture the improvement in density for the medium and fine, compared with the coarse, does not occur.

3.4 OTHER INTERACTIONS - DURABILITY

It can be seen from Table 3.2 that the durabilities at 30 per cent moisture are all very low and from a practical point of view would be unacceptable. Consideration has therefore been given to the results at 10 and 20 per cent moisture which produce acceptable pellets. The supplementary analysis of variance carried out on the results at 10 and 20 per cent is shown in Table 3.5.

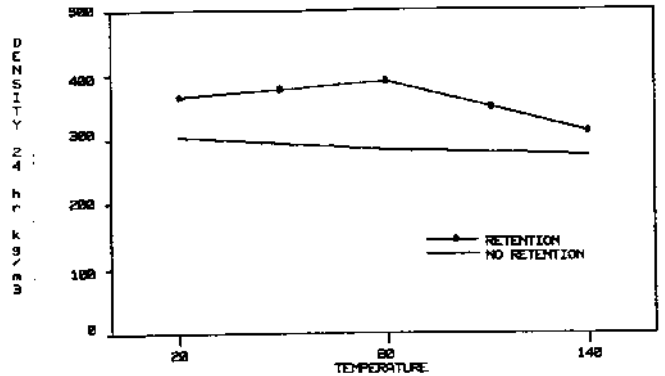

FIGURE 3.9 ILLUSTRATION OF TEMPERATURE-RETENTION INTERACTION

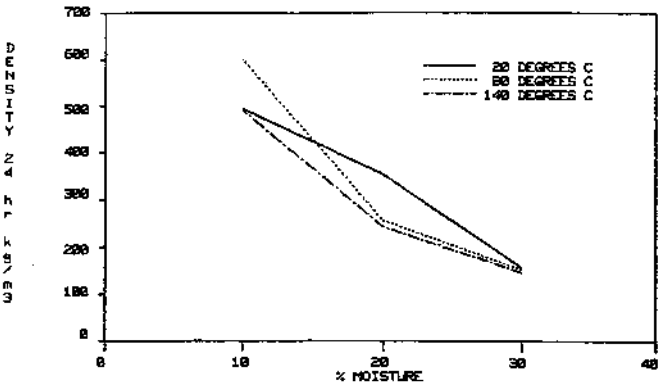

FIGURE 3.10 ILLUSTRATION OF MOISTURE-TEMPERATURE INTERACTION

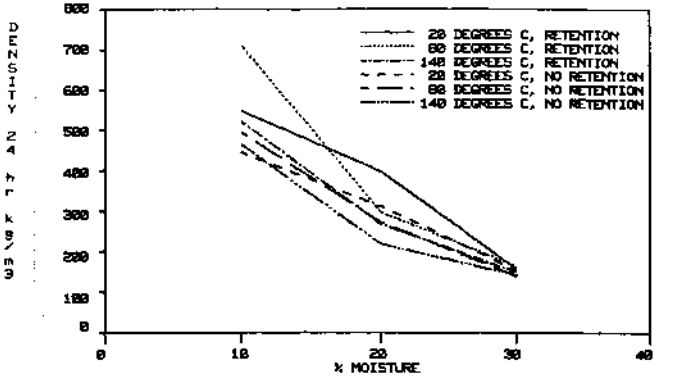

FIGURE 3.11 ILLUSTRATION OF MOISTURE-TEMPERATURE-RETENTION INTERACTION

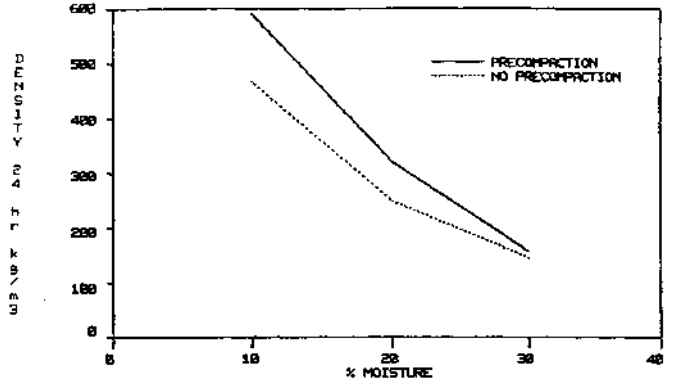

FIGURE 3.12 ILLUSTRATION OF MOISTURE-PRECOMPRESSION INTERACTION

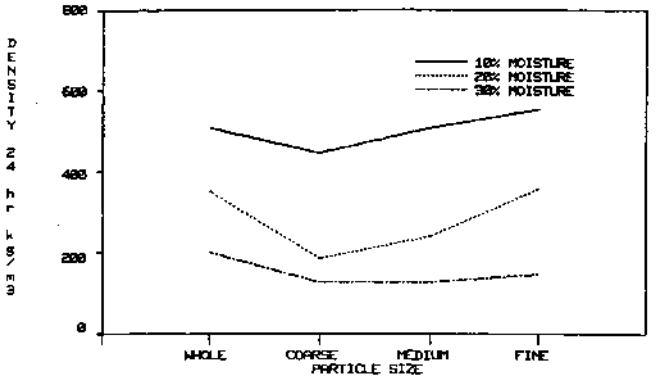

FIGURE 3.13 ILLUSTRATION OF PARTICLE SIZE-MOISTURE INTERACTION

TABLE 3.5 RESULTS OF ANALYSIS OF VARIANCE - DURABILITY 10 AND 15 PER CENT

Source	Degrees of Freedom	Variance Ratio	Significance Level
TOTAL	191		
T	2	15.404	Less than .001
W	1	373.329	Less than .001
C	1	149.585	Less than .001
X	1	273.499	Less than .001
M	3	204.529	Less than .001
TW	2	36.551	Less than .001
TC	2	4.538	.010 - .050
TX	2	2.775	.050 - .100
TM	6	24.001	Less than .001
WC	1	15.118	Less than .001
WX	1	51.040	Less than .001
WM	3	85.224	Less than .001
CX	1	27.318	Less than .001
CM	3	75.503	Less than .001
XM	3	14.641	Less than .001
TWC	2	10.287	Less than .001
TWX	2	12.128	Less than .001
TWM	6	6.710	Less than .001
TCX	2	0.111	
TCM	6	1.215	Greater than .250
TXM	6	2.329	.010 - .050
WCX	1	3.953	.010 - .050
WCM	3	8.231	Less than .001
WXM	3	13.214	Less than .001
CXM	3	5.553	.001 - .010
TWCX	2	2.536	.050 - .100
TWCM	6	4.561	Less than .001
TWXM	6	4.025	.001 - .010
TCXM	6	0.548	
WCXM	3	0.720	
TWCXM	6	0.680	
ERROR	96		

The CX interaction is outlined in Figure 3.14. This illustrates that precompression was relatively more beneficial when no retention was used.

The CM, MW and MT interactions are illustrated in Figures 3.15 to 3.17. These interactions are due to the relatively poorer performance of the coarse fraction at no precompression, higher moisture and lower temperature.

3.5 CONCLUSIONS

The tests carried out have extended the knowledge of bagasse compactions and durabilities from those previously reported in report 79/9389. The higher temperatures of 140° did not produce better performance than at 80°C.

The tests established that the best condition within the range tested for design of a pelleting machine would be:

Moisture of Bagasse	10 per cent
Temperature of Bagasse	80° C
Bagasse	Whole
Retention	500 kPa for 2 minutes
Precompression	Not necessary

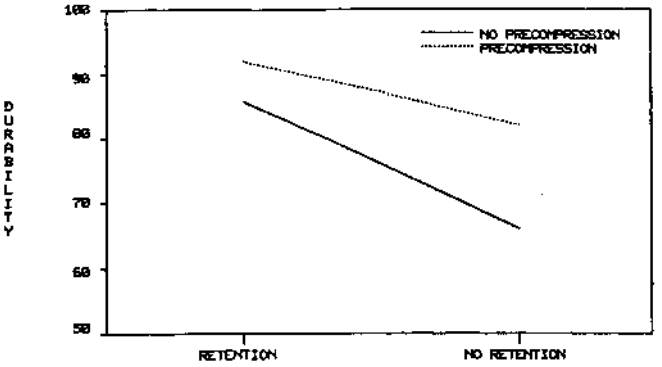

FIGURE 3.14 ILLUSTRATION OF RETENTION-PRECOMPRESSION INTERACTION

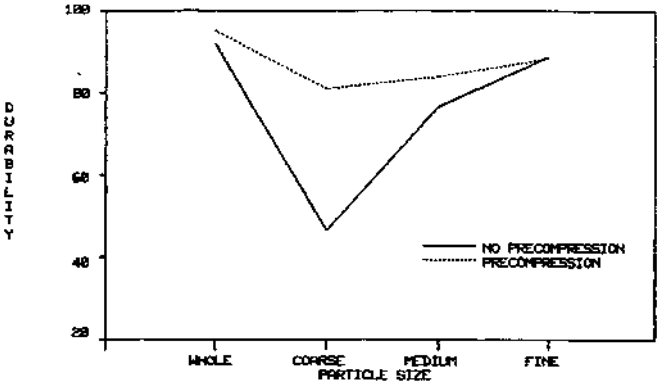

FIGURE 3.15 ILLUSTRATION OF PARTICLE SIZE-PRECOMPRESSION INTERACTION

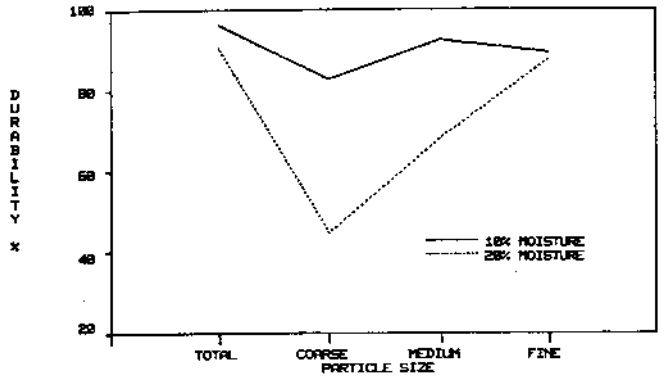

FIGURE 3.16 ILLUSTRATION OF PARTICLE SIZE-MOISTURE INTERACTION

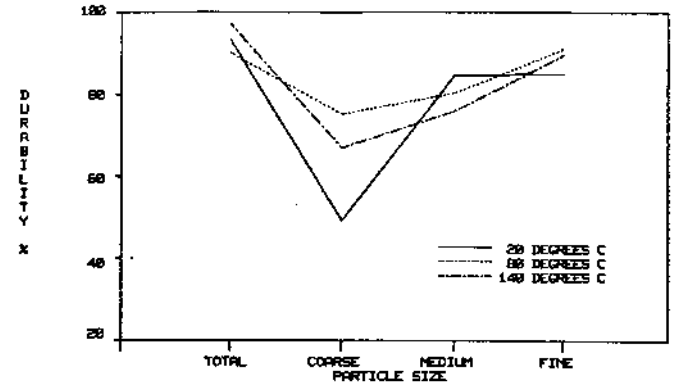

FIGURE 3.17 ILLUSTRATION OF PARTICLE SIZE-TEMPERATURE INTERACTION

CHAPTER 4
PROPERTIES OF SINGLE FIBRES

4.1 INTRODUCTION

The compaction characteristics of a mass of bagasse depend on the properties of the individual components that make up a sample. Very little work has been carried out to establish the basic properties of bagasse fibres so some preliminary experiments were carried out to evaluate these properties in an attempt to understand better the compression process for bagasse.

4.2 YIELD STRESS AND YOUNG'S MODULUS

A small rig was constructed which consisted of a beam arrangement where an individual fibre could be loaded at its mid point and deflections measured by means of a projection microscope. The basic gauge length used was 19 mm and fibres (or more precisely fibro vascular bundles) were selected at random. These ranged from typically .38 mm diameter up to larger beams of 1.7 x 1.45 mm and approximately oval in cross section.

The stress/strain relationships were established for the individual fibres and Figure 4.1 shows the relationship between applied bending stress and measured deflection of the beam. This test shows that initial yield occurs at stresses of approximately 54 MPa and with repeated loading significantly higher yield stresses were obtained. Figure 4.1 also illustrates significantly the hysteresis effect experienced with the bagasse fibres. The initial tests established that the stress/strain relationship was time dependent and tests were carried out to quantify the magnitude of the influence of time.

Figure 4.2 shows the relationships for bending stress and deflection of a beam when each load is applied for a 2 minute period. From this figure it can be seen how significant the hold time is. The results of tests on a range of fibres is

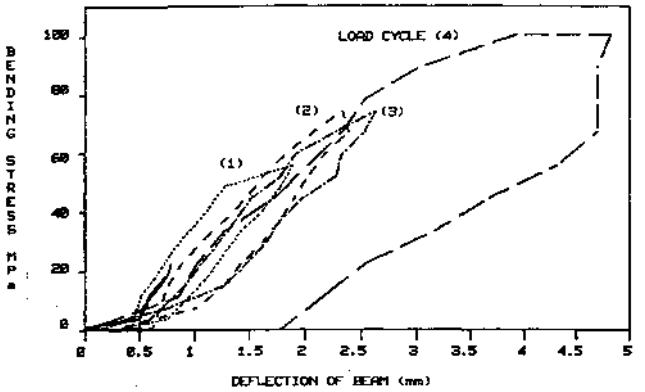

FIGURE 4.1 RELATIONSHIP BETWEEN DEFLECTION OF BEAM AND BENDING STRESS FOR SINGLE FIBRE

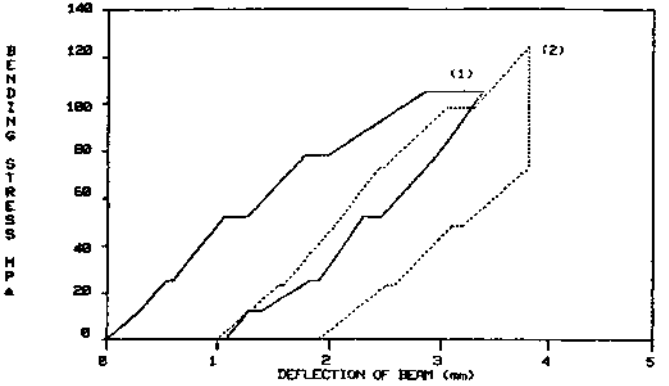

(1) 1ST APPLICATION OF LOAD
(2) 2ND APPLICATION OF LOAD

FIGURE 4.2 RELATIONSHIP BETWEEN DEFLECTION OF BEAM AND BENDING STRESS FOR INDIVIDUAL FIBRE. HOLD TIME BETWEEN SUCCESSIVE INCREASES IN BENDING MOMENT 2 MIN.

illustrated in Table 4.1. Yield stresses are seen to vary significantly for the fibres in the general diameter range .38 to .46 mm from 54 to 120 MPa. These yield stresses were recorded on the first loading.

Values of Young's modulus are seen to be reasonably consistent for the fibres in the range .38 to .43 mm diameter when the tests were conducted with a gauge length of 19 mm. However for the slightly larger diameter fibres with tests conducted on the 10.2 mm gauge length the values of Young's modulus that were established tended to be lower. The reasons for this have not been fully investigated.

It can also be seen from Table 4.1 that the larger fibro vascular pellets tested gave significantly lower value of yield stress and Young's modulus.

4.3 DENSITY OF FIBRES

Tests were carried out to determine the density of individual fibres and the results are shown in Table 4.1. Densities for the smaller fibres ranged from 711 to 719 kg/m^3 whilst the densities of the larger fibro vascular bundles ranges from 296 to 449 kg/m^3 . The relationship between Young's modulus and density was investigated and the results are shown in Figure 4.3. For the tests at 19 mm beam length there appears to be a reasonable linear relationship.

4.4 INFLUENCE OF FIBRE PROPERTIES ON PACKING THEORIES

The Van Wyk model was developed to investigate the packing characteristics of wool and preliminary tests by Loughran established that it could give an approximation to the compaction relationship for bagasse. The Van Wyk relationship as described by Loughran is:

TABLE 4.1 RESULTS OF TESTS ON SINGLE FIBRES

Fibre NO.	Fibre Diameter (mm)	Gauge Length (mm)	Yield Stress (MPa)	Ultimate Stress (MPa)	Youngs Modulus- MPa x 10^3	Density (kg/m^3)
1	.41	19	54		7.86	730
2	.38	19	120		8.13	870
3	.43	19	105		7.02	711
4	.46	10.2	90	110	5.08	879
6	1.7 x 1.45	19.3	28		1.24	449
8	1.45 x 1.17	19.3	25		1.00	296
9	.53	10.2	105	105	3.44	-

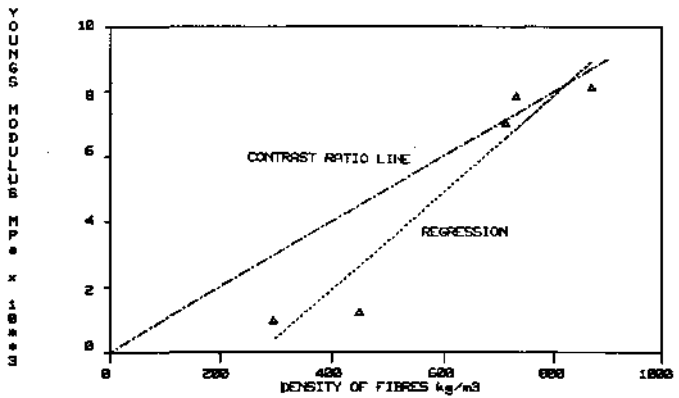

FIGURE 4.3 RELATIONSHIP BETWEEN DENSITY OF FIBRES AND YOUNG'S MODULUS

$$p = \frac{kE}{3} \frac{m^3}{f} \left(\frac{1}{v^3} - \frac{1}{v_0^3} \right)$$

p = Pressure (MPa)
k = Constant
E = Young's Modulus (MPa)
m = Mass charge (kg)
f = fibre density (kg/m^3)
v = Volume (m^{-3})
v_0 = Initial volume at p_0 (m^{-3})

The values of Young's Modulus and fibre density obtained in the tests outlined in Table 4.1 have been used to develop the pressure density relationship for bagasse fibres. This relationship is shown in Figure 4.4, The figure also shows the density versus pressure regression relationship for whole bagasse at 10 per cent moisture developed in the experimental work.

Whilst it can be seen that the forms of the equations are similar there is an obvious need for much more work under controlled conditions of temperature and moisture.

4.5 CONCLUSIONS

The work described in this section has been purely of a preliminary nature and has established the importance of time dependence on the stress/strain relationships for bagasse fibres. It has also highlighted the need for a more thorough investigation under controlled conditions before the Van Wyk theory can be tested rigorously for applicability to the bagasse compaction model.

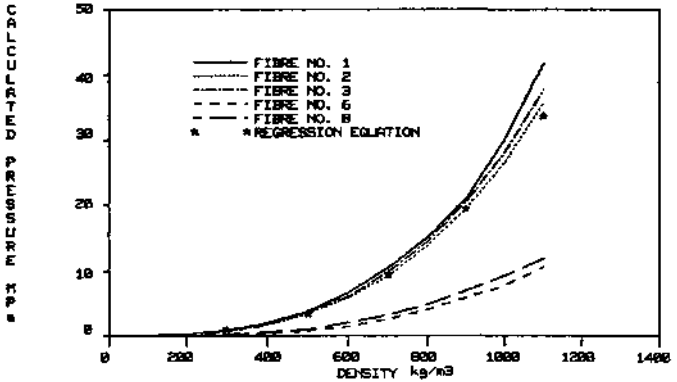

FIGURE 4.4 RELATIONSHIP BETWEEN DENSITY AND PRESSURE

CHAPTER 5
PRESSURE RELAXATION EFFECTS

5.1 INTRODUCTION

The basic aim of these experiments was to obtain an understanding of the retention mechanism by monitoring the load on and compaction of a sample of bagasse, both during compression and for a period afterwards, whilst the pellet's density was held constant.

The experiments were conducted using the INSTRON materials testing machine on which it is possible to control accurately the load or strain on, or displacement of a sample.

A summary of the specifications and the desirable operating ranges for these experiments appear in Tables 5.1 and 5.2. The apparatus used is shown in Figures 5.1 and 5.2.

The Instron was operated with position control for all the experiments. This control may be achieved either by using the Instron's own function generating circuits or by supplying a suitable signal from an external source. The internal ramp function was used for the constant velocity compression experiments. However, in order to achieve stability at the very low frequencies necessary for these tests, a Hewlett-Packard variable phase function generator with < 0.06 per cent distortion of the sinusoid was used.

The variables which were investigated are presented in Table 5.3.

The sinusoidal loading experiments were intended to simulate the compression speed experienced by a sample passing through a pair of rollers and then being held at the maximum compaction achieved at the nip.

TABLE 5.1 SUMMARY OF SPECIFICATION OF INSTRON

Load Rating,		± 250 kN dynamic
Speed Range,		30 mm sec^{-1}
Stroke		100 mm max
Load Ranges,	High	± 250 kN full scale
	Low	± 25 kN full scale

TABLE 5.2 DESIRABLE OPERATING RANGES

	High Range	Low Range
Nominal Height (mm)	80	80
Nominal Charge compaction in cylinders before compression (kg/m^3)	200	60
Maximum compaction for the range (kg/m^3)	1100	300
Height of pellet (mm)	14.5	16
Dry mass of fibre (g)	73	22
Estimated maximum load	185	3.75

TABLE 5.3 VARIABLES INVESTIGATED

Fibre fraction	coarse	fine	whole
Temperature ^{o}C	20	80	140
Moisture content wet basis (MCWB) %	10	20	30
Pellet density at compaction	300	800	1100
Type of loading	constant speed, sinusoidal*		
Speed* of compaction mms^{-1}	1.8	15	45
*The corresponding frequencies for the sinusoidal compactions are: (Hz)	0.0025	0.021	0.062

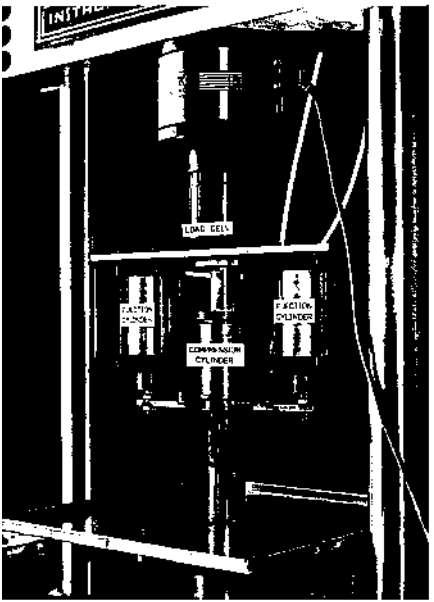

FIGURE 5.1 APPARATUS WITH COMPRESSION CYLINDER IN PLACE FOR A TEST.

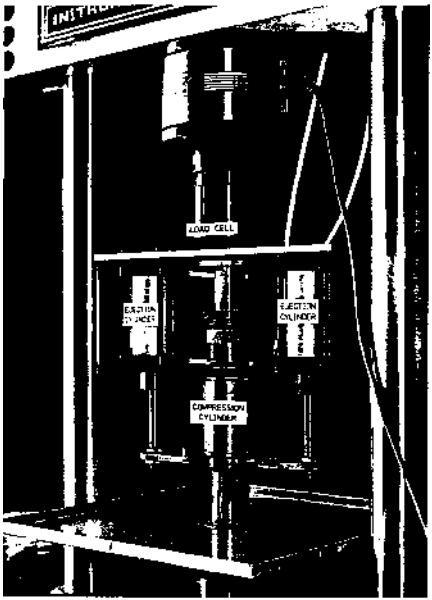

FIGURE 5.2 PELLET AFTER EJECTION OF COMPRESSION CYLINDER

It can be seen from Figure 5.3 that the height of a sample as it passes into a pair of rollers is given by

$$h = n + 2R(1 - \cos 0)$$

and the compression speed $V = \frac{dh}{dt}$

$$V = 2\ R \sin$$

It is at once obvious that only a portion of a sine wave is required for these experiments. Control was achieved by applying a D.C. offset and amplification to the signal from the H.P. function generator so that the required portion of the signal was suitable for use in controlling the position of the ram.

5.2 PREPARATION

Sufficient quantities of bagasse of the various fibre fractions and moisture contents were prepared. The Instron position controller was calibrated both for speed of compression and height of ram so that the height of a sample could be determined readily from the output voltage. Fortunately, the response was linear. It was found to be necessary to recalibrate the height after any accidental overloading of a sample to beyond the full dynamic load rating.

5.3 PROCEDURE

Compression cylinders were filled with a particular sample of bagasse and then sealed. Those containing samples which were to be tested at 80°C and 140°C were then placed in a preheated oven for two hours. After the sample had reached its designated temperature the sealed compression cylinder was placed in the test rig and the sample was compressed to the preset height. Both the position of the ram and the load on the pellet were monitored continuously and recorded on an electrostatic plotter. In order to obtain satisfactory resolution of the changes in load during and after the compaction the chart speeds were; 25 mm/s^{-1} during compression and for approximately 30 seconds after peak

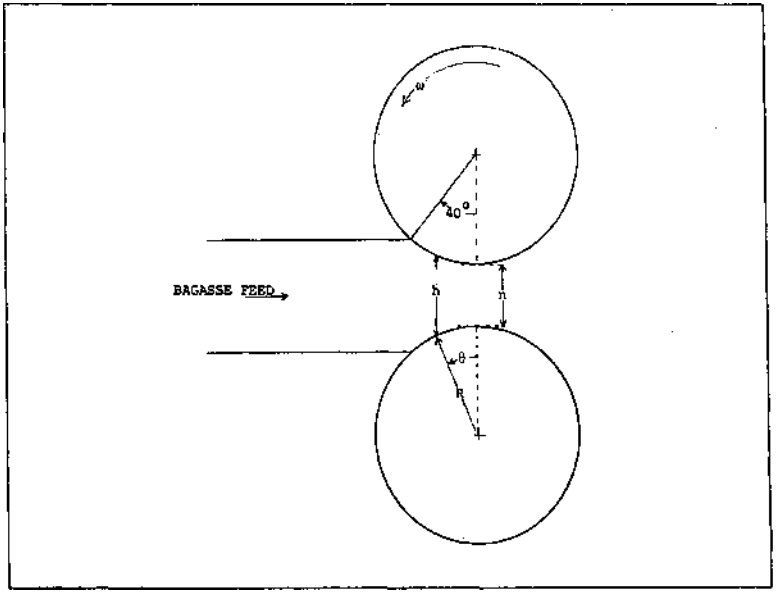

FIGURE 4.3 HEIGHT OF A SAMPLE PASSING THROUGH A PAIR OF ROLLERS

loading, 5 mm/s^{-1} for the next 30 seconds and thereafter intermittently at 30 second intervals for the remainder of the test.

After each test, the pellet was unloaded, the compression cylinder removed and the pellet's weight (80° and 140°C tests only), height and diameter were recorded. Further measurements of height and diameter were made at 24 hours. At 80°C and 140°C, the difference between the total mass of material placed in the cylinder and that of the pellet is largely a measure of the moisture loss during compression.

Some typical charts are shown in Figures 5.4 and 5.5. These illustrate the effect that the type and speed of loading has on the sample.

The following information was obtained from each chart:

Peak pressure (P)
Pressure after 2 minutes (P_{2min})
Rate of application of load (Lu)
Rate of relaxation of load (Ld)

The ratios P_{2mm}/P_{max} and Lu/Ld were also calculated.

5-4 RESULTS OF TESTS AT 10 PER CENT MOISTURE - LINEAR COMPACTION

A series of tests was carried out with bagasse at 10 per cent moisture to investigate the effect of the following variables on the dynamic compression characteristics of bagasse.

Temperature of compression T 20°C; 80°C; 140°C.
Material F Fine; Coarse; Whole.
Compaction C 300 kg/m^3; 800 kg/m^3; 1 100 kg/m^3.
Speed of compaction s 45 mm/s; 15 mm/s; 1.8 mm/s.

5.4.1 PEAK PRESSURE

The values obtained for the peak pressure are outlined in Table 5.4. The results of an analysis of variance on the results

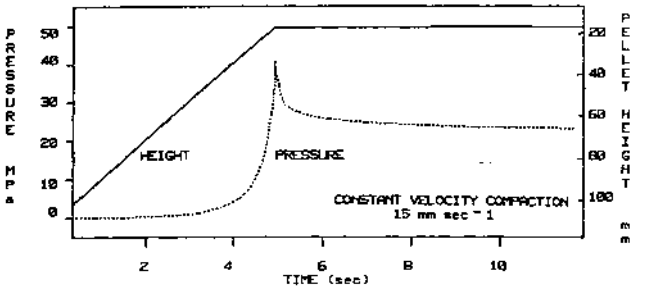

FIGURE 5-4 EFFECT OF HOLD TIME ON PRESSURE OF A PELLET AT CONSTANT HEIGHT - CONSTANT VELOCITY COMPACTION

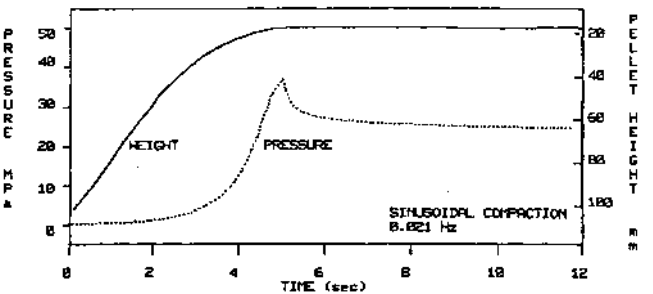

FIGURE 5.5 EFFECT OF HOLD TIME ON PRESSURE OF A PELLET AT CONSTANT HEIGHT - SINUSOIDAL COMPACTION

TABLE 5.4 PEAK PRESSURES OBTAINED (MPa) - 10% MOISTURE LINEAR COMPRESSION

		44 mm/s			15mm/s			1.8 mm/s		
Temp.	Comp.	Coarse	Fine	Whole	Coarse	Fine	Whole	Coarse	Fine	Whole
20°C	1 100	47.5	30.2	45.8	45.5	28.6	42.5	36.7	22.7	35.1
	800	15.72	8.80	14.1	14.8	9.1	13.3	12.83	8.22	12.0
	300	0.98	0.63	.800	0.97	0.64	.785	0.93	0.57	.674
80°C	1 100	41.25	26.6	29.6	42.76	21.93	32.1	34.82	21.1	24.84
	800	12.2	6.23	8.77	12.7	5.55	7.68	10.34	5.59	7.02
	300	.577	.511	.439	.555	.456	.458	.461	.423	.400
140°C	1 100	29.90	18.31	20.8	34.3	15.79	16.2	27.96	16.11	19.5
	800	7.13	3.07	3.90	6.91	3.83	5.66	6.21	3.84	5.26
	300	.559	.467	.425	.603	.482	.387	.526	.406	.362

are shown in Table 5.5. All factors are significant and the results are shown graphically in Figures 5.6 to 5.9. Peak pressure is seen to increase as speed of application increases and falls as temperature is increased in the range 20° to 140°C. The influence of particle size and compaction are as would be expected, peak pressure increasing as compaction increases and being lower for fine than for coarse material, with whole material being somewhere between coarse and fine. The results shown in these figures are averaged over all other variables.

Of the two-factor interactions the TC and FC interactions shown in Figures 5.10 and 5.11 are of most interest. These show that the effect of both temperature and material size is less as compaction is decreased.

5.4.2 RATIO OF PRESSURE AT 2 MIN TO PEAK PRESSURE

The values of the ratio P_{2min}/P_{max} which is a measure of the relaxation of the pressure are shown in Table 5.6 and the results of the analysis of variance are shown in Table 5.7. All of the prime variables are seen to have a significant effect on the ratio. The effects are shown graphically in Figures 5.12 to 5.15.

It can be seen that the pressure for the fine material falls slightly more than that for coarse and whole. Of particular interest is the fact that as the speed of compression increases, the smaller the relative value of pressure after two minutes. The relative value of pressure after two minutes is seen to decrease as temperature increases and increase as the level of compaction increases.

5-5 RESULTS OF TESTS AT 10% MOISTURE - SINUSOIDAL COMPACTION

Tests were carried out to determine the effect of method of compression - sinusoidal or linear - on the compression characteristics of bagasse. Tests were confined to whole bagasse and were carried out under the following conditions.

TABLE 5.5 RESULTS OF ANALYSIS OF VARIANCE - PEAK PRESSURES

Source	Degrees of Freedom	Variance Ratio	Significance Level
TOTAL	80		
S	2	22.687	Less than .001
F	2	179.738	Less than .001
T	2	204.934	Less than .001
C	2	3487.325	Less than .001
SF	4	1.725	.100 - .250
ST	4	3.724	.010 - .050
SC	4	12.457	Less than .001
FT	4	9.170	Less than .001
FC	4	78.115	Less than .001
TC	4	73.784	Less than .001
SFT	8	0.477	
SFC	8	1.335	Greater than .250
STC	8	2.448	.050 - .100
FTC	8	6.026	.001 - .010
SFTC	16	1.000	Greater than .250
ERROR	16		

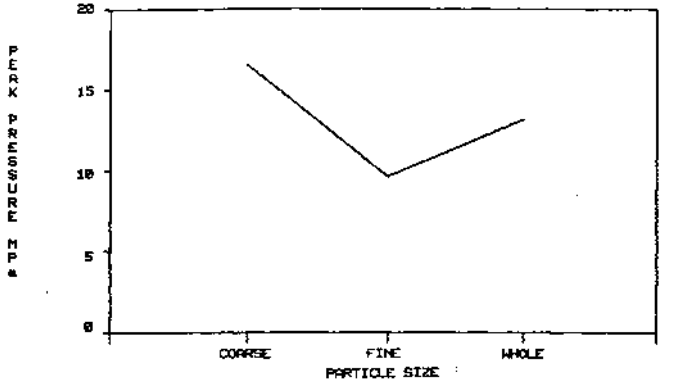

FIGURE 5-6 RELATIONSHIP BETWEEN PARTICLE SIZE AND PEAK PRESSURE

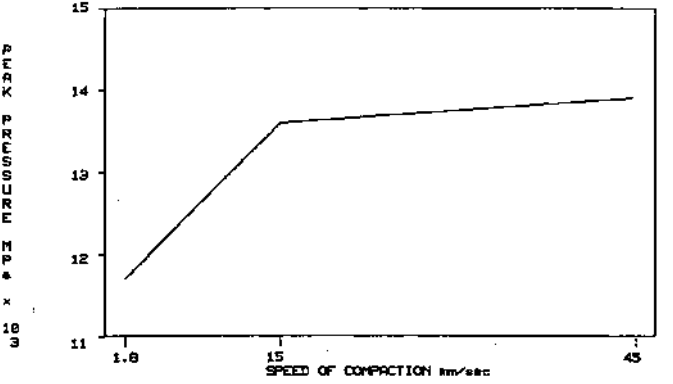

FIGURE 5-7 RELATIONSHIP BETWEEN SPEED OF COMPACTION AND PEAK PRESSURE

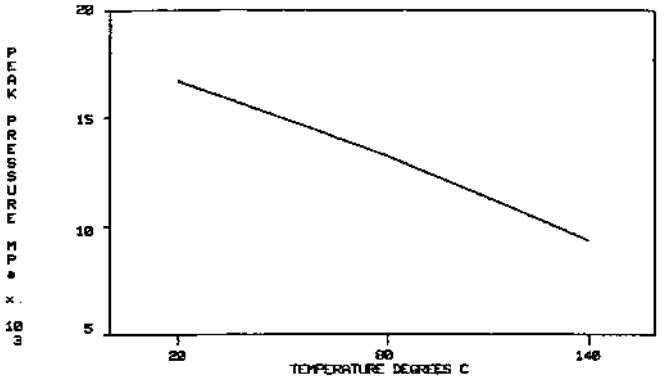

FIGURE 5.8 RELATIONSHIP BETWEEN TEMPERATURE AND PEAK PRESSURE

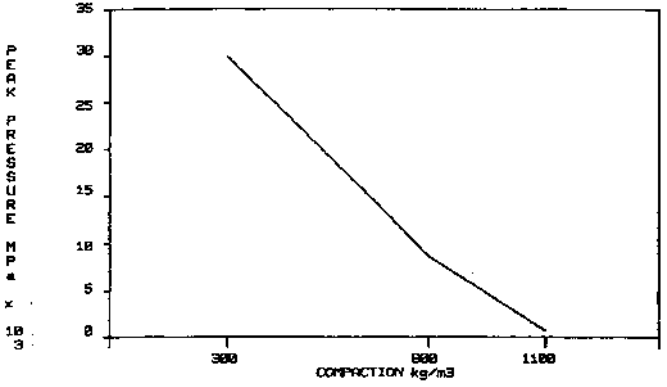

FIGURE 5.9 RELATIONSHIP BETWEEN COMPACTION AND PEAK PRESSURE

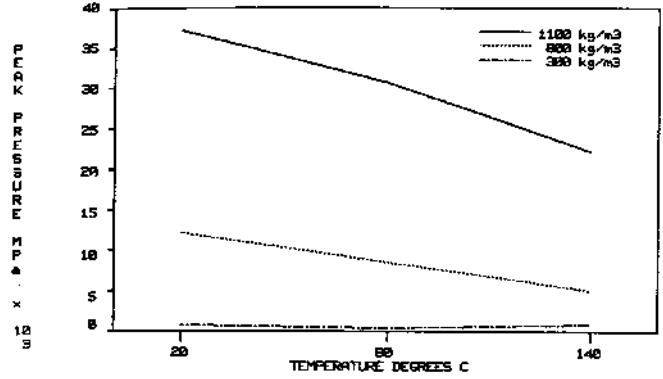

FIGURE 5.10 ILLUSTRATION OF TEMPERATURE-COMPACTION INTERACTION

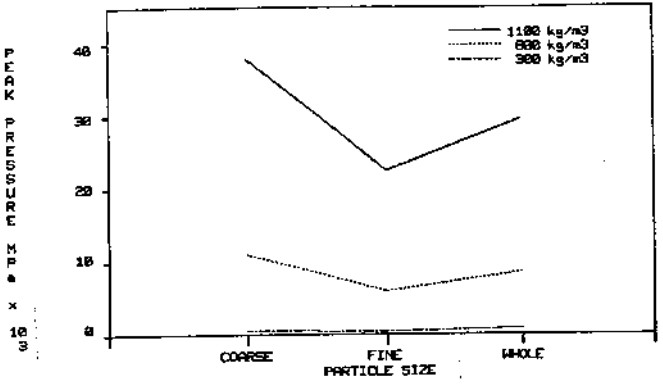

FIGURE 5.11 ILLUSTRATION OF PARTICLE SIZE-COMPACTION INTERACTION

TABLE 5.6 RESULTS OF RATIO P_{2min}/P_{max}

		44 mm/S			15 mm/S			1.8 mm/s		
Temp.	Comp.	Coarse	Fine	Whole	Coarse	Fine	Whole	Coarse	Fine	Whole
20°C	1 100	.444	.391	.435	.488	.455	.490	.567	.542	.618
	800	.402	.354	.364	.437	.398	.430	.530	.52	.523
	300	.413	.397	.332	.449	.456	.427	.494	.538	.475
80°C	1 100	.359	.289	.352	.417	.325	.402	.532	.533	.512
	800	.302	.238	.288	.344	.287	.343	.465	.392	.469
	300	.285	.227	.288	.308	.255	.289	.419	.415	.479
140°C	1 100	.266	.228	.289	.344	.264	.305	.471	.415	.493
	800	.262	.167	.213	.286	.214	.283	.435	.357	.417
	300	.196	.178	.193	.229	.227	.241	.354	.314	.326

TABLE 5.7 RESULTS OF ANALYSIS OF VARIANCE OF P_{2MIN}/P_{MAX}

Source	Degrees of Freedom	Variance Ratio	Significance Level
TOTAL	80		
S	2	525.701	Less than .001
F	2	35.133	Less than .001
T	2	486.364	Less than .001
C	2	109.914	Less than .001
SF	4	1.327	Greater than .250
ST	4	5.204	.001 - .010
SC	4	2.274	.100 - .250
FT	4	4.216	.010 - .050
FC	4	4.910	.001 - .010
TC	4	4.244	.010 - .050
SFT	8	0.726	
SFC	8	0.471	
STC	8	1.283	Greater than .250
FTC	8	1.982	.100 - .250
SFTC	16	1.000	Greater than .250
ERROR	16		

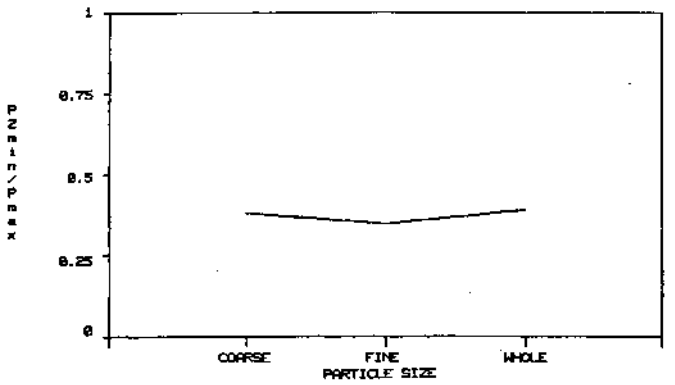

FIGURE 5.12 EFFECT OF PARTICLE SIZE ON RATIO P_{2MIN}/P_{MAX}

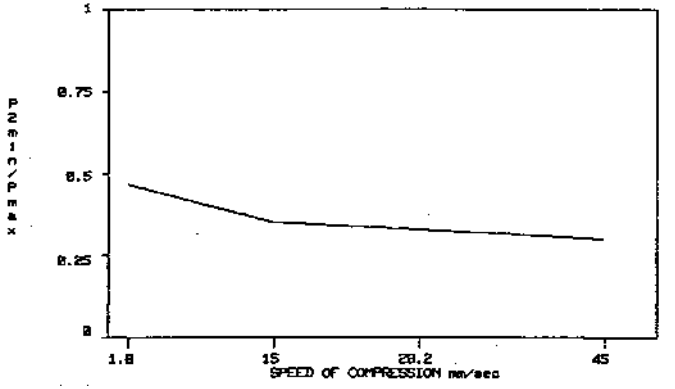

FIGURE 5.13 EFFECT OF SPEED ON RATIO P_{2MIN}/P_{MAX}

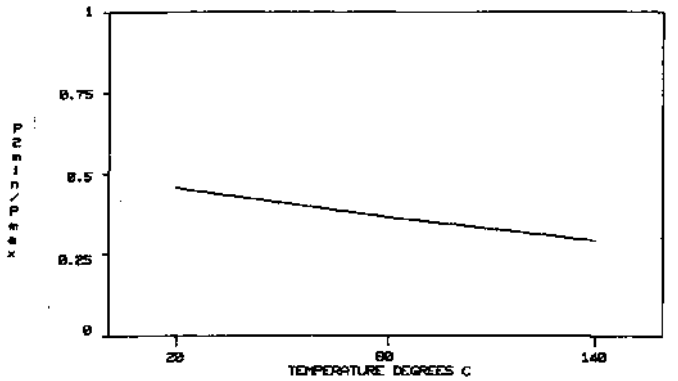

FIGURE 5.14 EFFECT OF TEMPERATURE ON RATIO P_{2MIN}/P_{MAX}

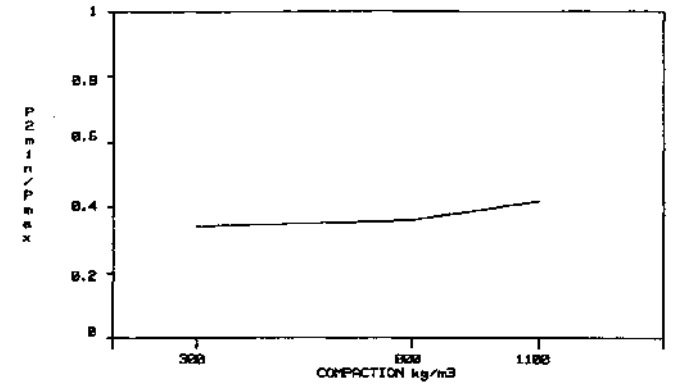

FIGURE 5.15 EFFECT OF COMPACTION ON RATIO P_{2MIN}/P_{MAX}

Type of Compression	L	Linear; Sinusoidal.
Speed of Compression	S	45 mm/s; 15 mm/s; 1.8 mm/s.
Temperature	T	20°C; 80°C; 140°C.
Compression	C	300 kg/m^3; 800 kg/m^3; 1 100 kg/m^3.

5.5.1 PEAK PRESSURE

The results of peak pressure obtained from the tests are shown in Table 5.8 and the analysis of variance of the results is shown in Table 5.9. As expected from previous tests there is a significant effect of level of compaction and temperature but it was found that speed of compression was of limited significance and that the effect of type of loading was significant only at the 0.05 level with the sinusoidal type of loading giving slightly lower maximum pressures as shown in Table 5.10. The TC interaction discussed in 5.4.1 is again evident.

TABLE 5.10 AVERAGE PEAK PRESSURES MPa

Sinusoidal	Linear
11.9	13.0

5.5.2 RATIO OF PRESSURE AT 2 MIN TO P_{max}

The results obtained for the tests are shown in Table 5.11 and the analysis of variance results are shown in Table 5.12. The effects of temperature , compaction and speed are similar to those outlined in Figures 5.13 to 5.15. The effect of type of loading is shown in Table 5.11.

TABLE 5.8 VALUES OF PEAK PRESSURE MPa

		Linear			Sinusoidal		
Speed (mm/s)		45	15	1.8	45	15	1.8
20°C	1 100	45.8	42.5	35.1	36.3	39.2	37.4
	800	14.1	13.3	12.0	12.8	11.8	9.98
	300	.797	.781	.672	.797	5.73	.684
80°C	1 100	29.6	32.1	24.8	2 9.1	26.0	24.6
	800	8.77	7.68	7.02	7.68	6.54	6.33
	300	.438	.457	.398	.375	.402	.414
140°C	1 100	20.8	16.2	19.5	17.9	16.5	17.8
	800	3.9	5.66	5.26	3.76	4.22	4.66
	300	.422	3.87	.359	.285	.328	2.93

TABLE 5.9 RESULTS OF ANALYSIS OF VARIANCE P_{MAX} SINUSOIDAL VS LINEAR COMPACTION

Source	Degrees of Freedom	Variance Ratio	Significance Level
TOTAL	53		
L	1	4.205	.050 - .100
S	2	3.096	.100 - .250
T	2	110.659	Less than .001
C	2	900.947	Less than .001
LS	2	0.589	
LT	2	0.000	
LC	2	1.767	.100 - .250
ST	4	1.110	Greater than .250
SC	4	1.281	Greater than .250
TC	4	40.836	Less than .001
LST	4	0.825	
LSC	4	0.717	
LTC	4	0.609	
STC	8	0.749	
LSTC	8	1.000	Greater than .250
ERROR			

TABLE 5.11 VALUES OF P_{2min}/P_{max}

		Linear			Sinusoidal		
Speed (mm/s)		45	15	1.8	45	15	1.8
20°C	1 100	.435	.490	.618	.513	.545	.606
	800	.364	.430	.523	.410	.481	.560
	300	.332	.427	.475	.468	.498	.532
80°C	1 100	.352	.402	.512	.415	.468	.598
	800	.288	.343	.469	.386	.419	.502
	300	.288	.289	.479	.290	.345	.447
140°C	1 100	.289	.305	.493	.368	.419	.549
	800	.213	.283	.417	.306	.351	.435
	300	.193	.241	.326	.209	.264	.436

TABLE 5.12 RESULTS OF ANALYSIS OF VARIANCE OF P_{2MIN}/P_{MAX}

Source	Degrees of Freedom	Variance Ratio	Significance Level
TOTAL	53		
L	1	46.121	Less than .001
S	2	124.370	Less than .001
T	2	99.090	Less than .001
C	2	50.524	Less than .001
LS	2	1.152	Greater than .250
LT	2	0.242	
LC	2	0.310	
ST	4	1.731	.100 - .250
SC	4	0.289	
TC	4	1.363	Greater than .250
LST	4	0.406	
LSC	4	0.228	
LTC	4	1.614	Greater than .250
STC	8	0.449	
LSTC	8	1.000	Greater than .250
ERROR			

TABLE 5.13 AVERAGE VALUES OF P_{2min}/P_{max}

Sinusoidal	Linear
.438	.381

5.6 CONCLUSIONS

The results presented in this section have given a basic understanding of the relaxation properties of bagasse. The relaxation properties are of particular importance in the rolling action type of pelleter machine where the material is compressed by moving it through a gap of fixed dimensions and not at constant pressure. Because of this tendency for pressure to fall off, thus reducing hold time and potentially pellet density it is important that pressure in the horizontal direction i.e. at right angles to roll pressure applied vertically, to be maintained. The controlling influence on force in the horizontal direction is coefficient of friction. This will be discussed in Chapter 7.

CHAPTER 6
ENERGY OF COMPACTION

6-1 INTRODUCTION

The energy required to compact a sample of bagasse is of prime importance in the design of a compacting machine. Tests were therefore carried out to determine the energy of compaction, not only of the first compression stroke but on subsequent strokes up to the tenth compression. The tests were carried out on the equipment shown in Figures 5.1 and 5.2.

6-2 SCOPE OF TESTS

Two series of tests were carried out, the first series was at the following conditions:

Speed	S	15 mm/s .094 Hz; 11.8 mm/s .0013 Hz
Moisture	M	10%; 20%; 30%.
Material	F	Coarse, Fine, Whole.
Compaction	C	1 100 kg/m^3; 800 kg/m^3; 300 kg/m^3.
Replication	R	2

This gave a series of 108 tests.

The second series was carried out to investigate the effect of temperature. The variables investigated in this series were:

Temperature	T	20°C; 80°C; 140°C.
Moisture	M	10%; 20%; 30%.
Material	F	Coarse, Fine, Whole.
Compaction	C	1 100 kg/m^3; 800 kg/m .

This gave a total of 54 tests.

6-3 RESULTS

The form of the curves obtained for the tests is shown in Figure 6.1. The areas under the curves were found by integration using digital techniques on the recorded data and the energies were calculated in kJ/kg. Results of the tests are shown in Tables 6.1, 6.2 and 6.3.

6.3.1 INFLUENCE OF VARIABLES ON TESTS AT 20°C - 1ST COMPACTION

The results of the analysis of variance are shown in Table 6.4. It can be seen from this table that all of the factors investigated had a significant effect on the energy of compaction. The results averaged over other variables are shown in Figures 6.2 to 6.5. It can be seen from the results that:

Increases in compaction increase the energy required for compaction.

Increase in moisture content reduces the energy required for compaction.

Fine material requires significantly less energy for compaction than whole or coarse material.

An increase in speed increases the energy required for compaction.

Four of the two-factor interactions are significant. The most significant of these is the FC interaction shown in Figure 6.6. The MC interaction which is also significant, is shown in Figure 6.7. This shows how the difference between the energy required for compaction at different moistures increases as compaction increases.

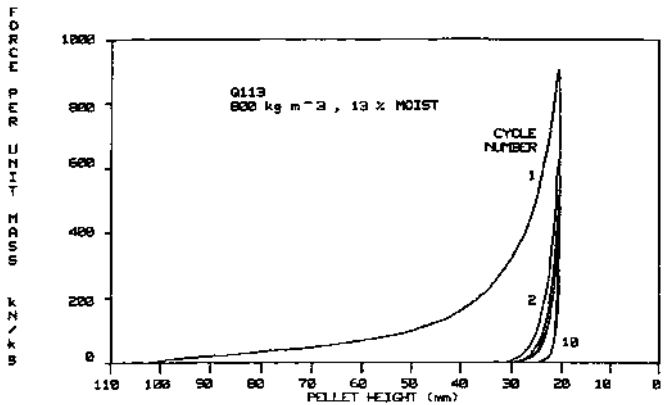

FIGURE 6.1 TYPICAL HYSTERESIS CURVES FOR BAGASSE

TABLE 6.1 ENERGY OF COMPACTION - 1ST CYCLE (kJ/kg)
TESTS AT 20°C

			Compression Speed					
			15 mm/s .094 H_z			1.8 mm/s .0113 H_z		
Moist %	Comp$_3$ kg/m^3	Rep	Coarse	Fine	Whole	Coarse	Fine	Whole
10	1 100	R_1	16.65	8.183	15 05	16 67	8.467	12.52
		R_2	15.68	9.01	15.03	16.03	8.202	12.06
	800	R_1	9.287	4.037	8.336	8.779	4.846	7.111
		R_2	6.562	5.013	8.377	8.865	4.840	7.428
	300	R_1	1.456	0.937	1.235	1.293	0.716	0.929
		R_2	0.347	0.227	1.330	1.473	1.411	1.075
20	1 100	R_1	14.28	7.434	10.39	13.22	7.043	9.229
		R_2	13.72	7.606	10.92	12.49	6.681	9.479
	800	R_1	6.826	3.357	5.215	7.471	2.893	4.951
		R_2	6.652	3.309	5.172	8.088	3.010	5.158
	300	R_1	1.356	0.539	0.931	1.053	0.505	0.741
		R_2	1.719	0.486	0.896	1.321	0.478	0.688
30	1 100	R_1	11.08	4.196	8.853	9.346	3.948	7.001
		R_2	11.66	7.397	8.588	8.905	3.530	6.853
	800	R_1	6.155	2.309	5.319	5.315	2.206	4.185
		R_2	6.288	4.137	4.881	6.546	2.009	4.204
	300	R_1	1.083	0.518	0.677	0.925	0.405	0.581
		R_2	0.323	0.199	0.554	0.785	0.463	0.545

TABLE 6.2 ENERGY OF COMPACTION - 10TH CYCLE (kj/kg)
TESTS AT 20°C

			Compression Speed					
			15 mm/s .094 H_z			1.8 mm/s .0113 H_z		
Moist %	Comp kg/m^3	Rep	Coarse	Fine	Whole	Coarse	Fine	Whole
10	1 100	R_1	0.9308	0.3773	0.9113	1.750	0.5007	0.7781
		R_2	1.137	0.383	0.8754	1.332	0.4484	0.9854
	800	R_1	0.479	0.1374	0.3538	0.416	0.0022	0.2712
		R_2	0.479	0.233	0.362	0.407	0.1915	0.2911
	300	R_1	0.06-2	-	0.0237	0.0662	-	0.0168
		R_2	0.0063	0.0007	0.0399	0.0799	0.0457	0.0494
20	1 100	R_1	0.9238	0.5786	1.187	1.468	0.6982	0.9607
		R_2	0.6769	0.5867	0.8592	1.147	0.6519	1.065
	800	R_1	0.4417	0.1849	0.4064	0.7553	0.1727	0.453
		R_2	0.3573	0.1948	0.4188	0.6199	0.1879	0.357
	300	R_1	0.0741	0.0013	0.0572	0.0968	0.0093	0.0516
		R_2	0.4865	0.0064	0.0490	0.0456	0.0093	0.0316
30	1 100	R_1	0.4445	0.2101	0.7939	0.8037	0.2628	0.7452
		R_2	1.260	0.562	0.8118	0.7797	0.3087	0.5007
	800	R_1	0.1905	0.1027	0.5110	0.6045	0.1420	0.3435
		R_2	0.657	0.301	0.5125	0.7957	0.1155	0.3964
	300	R_1	0.0822	-	0.0573	0.1458	-	0.0515
		R_2	0.0182	0.0012	0.0489	0.1458	-	0.0544

TABLE 6.3 ENERGY COMPACTION - 1ST CYCLE (kJ/kg) - RESULTS AT 15 mm/s .094 H_z

		20°C			80°C			140°C		
Moist %	Comp kg/m^3	Coarse	Fine	Whole	Coarse	Fine	Whole	Coarse	Fine	Whole
10	1 100	16.65	8.183	15.05	12.11	5.237	8.090	7.982	3.013	6.566
	800	9.287	4.037	8.336	6.25	2.505	4.020	4.162	1.436	2.840
20	1 100	14.28	7.434	10.39	8.114	3.932	6.596	5.809	2.847	3.336
	800	6.826	3.357	4.215	3.667	1.796	2.499	2.305	1.075	1.962
30	1 100	11.08	4.196	8.853	6.596	6.944	2.421	6.452	5.465	3.180
	800	6.155	2.309	5.319	2.499	3.541	1.233	1.764	1.005	1.310

TABLE 6.4 RESULTS OF ANALYSIS OF VARIANCE - ENERGY OF 1ST CYCLE 20°C

Source	Degrees of Freedom	Variance Ratio	Significance Level
TOTAL	107		
S	1	22.450	Less than .001
F	2	395.072	Less than .001
M	2	223.750	Less than .001
C	2	2665.840	Less than .001
SF	2	5.116	.001 - .010
SM	2	4.112	.010 - .050
SC	2	16.433	Less than .001
FM	4	6.066	Less than .001
FC	4	91.691	Less than .001
MC	4	58.647	Less than .001
SFM	4	2.874	.010 - .050
SFC	4	1.224	Greater than .250
SMC	4	1.342	Greater than .250
FMC	8	2.323	.010 - .050
SFMC	8	0.641	
ERROR	54		

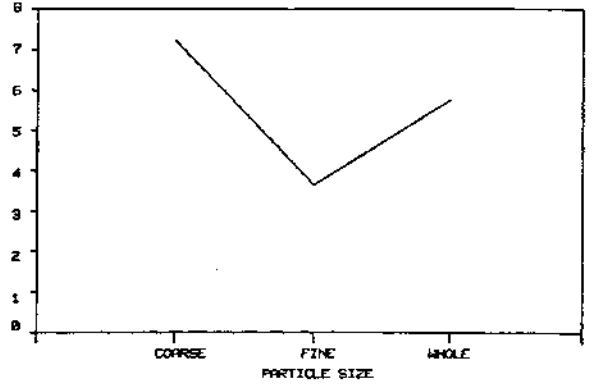

FIGURE 6.2 INFLUENCE OF PARTICLE SIZE ON ENERGY OF COMPACTION

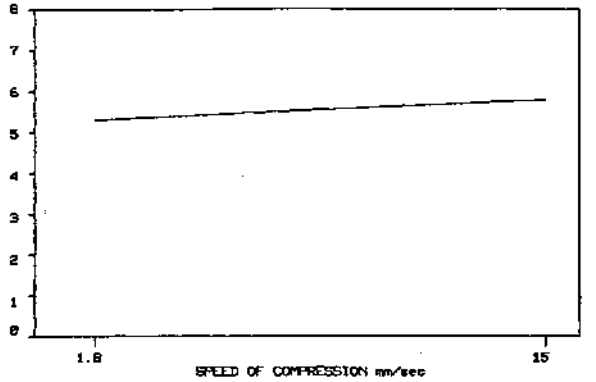

FIGURE 6.3 INFLUENCE OF SPEED OF COMPRESSION ON ENERGY OF COMPACTION

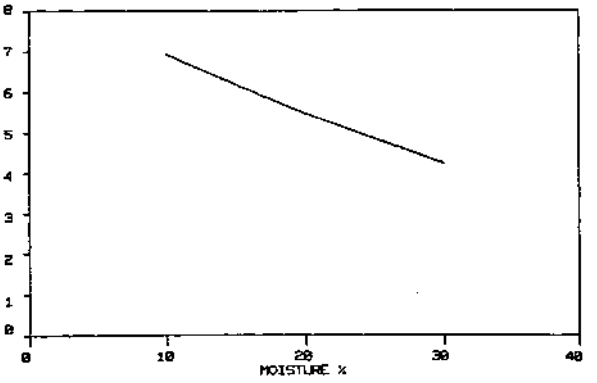

FIGURE 6.4 INFLUENCE OF MOISTURE ON ENERGY OF COMPACTION

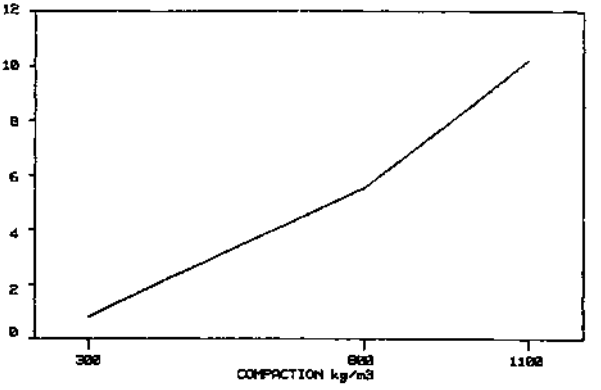

FIGURE 6.5 INFLUENCE OF COMPACTION LEVEL ON ENERGY OF COMPACTION

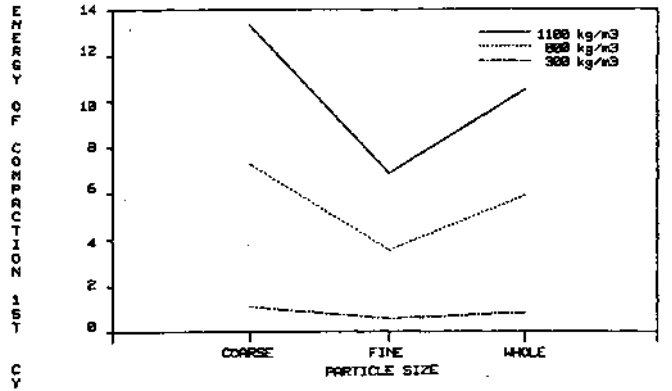

FIGURE 6.6 ILLUSTRATION OF PARTICLE SIZE-COMPACTION INTERACTION

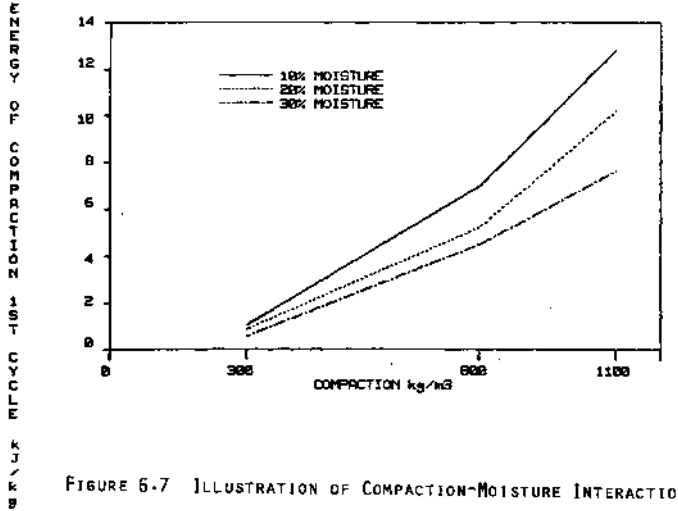

FIGURE 6.7 ILLUSTRATION OF COMPACTION-MOISTURE INTERACTION

6.3.2 INFLUENCE OF VARIABLES ON TESTS AT 20°C - 10TH COMPACTION

The results of the analysis of variance of the energies of compaction for the 10th cycle are shown in Table 6.5. These results in general show the same trends as the energy for the 1st cycle but the effects are less significant.

Average results of the ratio of the energy for the 10th cycle to the energy for the 1st cycle are shown in Table 6.6.

TABLE 6.6 RATIO OF ENERGY AT 10TH COMPACTION TO ENERGY AT 1ST COMPACTION

	Compaction (kg/m^3)		
	300	800	1 100
Ratio	.0781	.0643	.0632

6.3.3 EFFECT OF TEMPERATURE ON ENERGY OF COMPACTION

The results of the tests carried out to determine the effect of temperature on energy of compaction at higher levels of compaction are shown in Table 6.3. The results of the analyses of variance carried out on the results of these tests are shown in Table 6.7. The material size, moisture and compaction are all significant, together with the FM and FC interactions, as would be expected from the previous results.

Figure 6.8 illustrates the effect of temperature on energy of compaction. Increases in temperature are seen to significantly reduce compaction energy requirements.

Figure 6.9 illustrates the TF interaction. This shows that the difference between compaction energies for the range of material sizes is greater at 20°C than at 80° or 140 C.

TABLE 6.5 RESULTS OF ANALYSIS OF VARIANCE ON ENERGY OF COMPACTION FOR 10TH CYCLE

Source	Degrees of Freedom	Variance Ratio	Significance Level
TOTAL	107		
S	1	1.588	.100 - .250
F	2	61.903	Less than .001
M	2	4.724	.010 - .050
C	2	277.321	Less than .001
SF	2	5.603	.001 - .010
SM	2	1.130	Greater than .250
SC	2	1.396	Greater than .250
FM	4	0.522	
FC	4	10.710	Less than .001
MC	4	6.108	Less than .001
SFM	4	0.006	
SFC	4	2.027	.100 - .250
SMC	4	2.942	.010 - .050
FMC	8	1.696	.100 - .250
SFMC	8	1.039	Greater than .250
ERROR	54		

TABLE 6.7 RESULTS OF ANALYSIS OF VARIANCE OF TESTS AT DIFFERENT TEMPERATURES - ENERGY AT 1ST CYCLE

Source	Degrees of Freedom	Variance Ratio	Significance Level
TOTAL	53		
T	2	341.910	Less than .001
F	2	185.324	Less than .001
M	2	102.238	Less than .001
C	1	658.535	Less than .001
TF	4	26.888	Less than .001
TM	4	10.087	.001 - .010
TC	2	16.541	.001 - .010
FM	4	20.732	Less than .001
FC	2	19.360	Less than .001
MC	2	4.575	.010 - .050
TFM	8	5.490	.010 - .050 1
TFC	4	1.607	Greater than .250
TMC	4	4.884	.010 - .050
FMC	4	2.986	.050 - .100
TFMC	8	1.000	Greater than .250
ERROR	8		

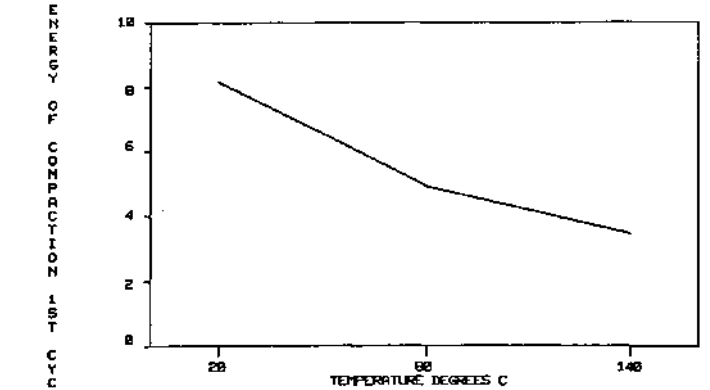

FIGURE 6.8 INFLUENCE OF TEMPERATURE ON ENERGY OF COMPACTION

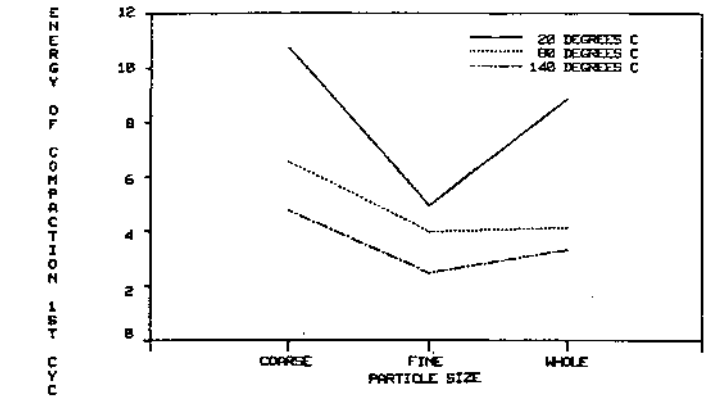

FIGURE 6.9 ILLUSTRATION OF PARTICLE SIZE-TEMPERATURE INTERACTION

6.4 CONCLUSIONS

The tests carried out to determine compression energy have quantified the influence of the different parameters. From a practical pelleting point of view the desirability of high temperatures and fine materials have been demonstrated. However the tests described in Chapter 5 have illustrated that the durability of fine material is not as good as that for the whole material.

It is interesting to consider the values of compression energy in relation to energies recorded in practical pelleting machines. The comparison is shown in Table 6.9 where it is seen that the energy to actually compress the fibres is a small fraction of total energy absorbed and therefore there is significant potential to reduce energy usage in operating machines.

TABLE 6.9 ENERGY REQUIRED TO PELLET BAGASSE

Condition	Energy kJ/kg Dry Matter
Drying Energy 50% to 10% Moisture	2 300
Theoretical	
Compression Energy (from U of Q)	2.3 - 10.7
Extrusion Energy in Dies	25
Actual	
Rotating Die - Jaybee	180 - 900
Slow Speed Extrusion - Haussman	180

CHAPTER 7
A THEORY OF BAGASSE COMPACTION

In this chapter the results of tests on individual bagasse fibre bundles are combined with a theory of the collective behaviour of many bagasse filaments in an attempt to relate the bulk properties of bagasse to individual filament properties.

7.1 BAGASSE FILAMENTS - STRESS-STRAIN RELATIONSHIP

As described in Chapter 4, tests were conducted on single filaments of bagasse, supported on two knife edge supports and loaded as shown.

Typical stress-deflection curves obtained in these tests are presented in Figure 4.1. For relatively low maximum stress levels, the loading and unloading curves lie close to one another implying that the material in the beam is behaving nearly elastically. However, as maximum stress levels are increased. the unloading curve is displaced to the right, implying that yield has taken place. For a given fibre, near maximum stress, increased deflection occurs with only small increases and in fact, most of the yield occurs at these stress levels. This behaviour can be idealized as a linear elastic relation between stress and strain up to a yield value, at which further non-elastic deflection occurs at constant stress.

However, it is well known that cellulose based materials, such as bagasse, also tend to exhibit creep i.e. under constant stress, strain increases with time. Thus the tests above were modified to allow 2 minute periods for creep relaxtion at selected stress levels. Figure 4.2 shows that creep does indeed take place, with deflection increasing with stress levels. Creep recovery also takes place during the unloading process but recovery is not complete -i.e. some part of the creep is elastic, and some represents yield. This behaviour, can be idealized by assuming that creep takes place at a

rate proportional to stress, that it is elastic up the yield stress, but creep taking place at yield is non-elastic, leading to permanent deformation. Also, as the second cycle in the Figure shows, if deflection in the beam is restrained when it is in the yield region, then creep takes place as a reduction in stress, but this still leads to an overall permanent deformation when the beam is unloaded.

Observation of a creep phenomenon raises the question of the relationship between stress and strain under more rapid loading conditions. This is particularly relevant to operation of a rolling type compaction apparatus, since the time spent in the nip of a pair of rollers is likely to be of the order of seconds, whilst the time for a complete cycle to produce the stress-strain curves of Figure 4.1 was of the order of 2 to 3 minutes. Thus the experiments reported in Appendix A were undertaken. Here the beam formed by the bagasse filament was loaded rapidly by applying the weight suddenly, and observing the resultant deflection of the beam by multiple flash photography.

Results are shown in Figure A.3. The filaments which did not rupture provide a stress-deflection curve which, because of elastic rebound of the beam, included part of an unloading curve. It can be seen that the cycle is qualitatively similar to that obtained with the much longer loading times associated with Figure 4.1, and can be idealized in the same way. The time for the complete cycle in these experiments was of the order of 0.1 sec, implying that the idealized model can be applied over a range of times which includes those appropriate to a rolling operation.

The concepts arising from these experiments lead to an idealized description of the behaviour of a filament, acting as a beam, which is part of an assembly subjected to compression. Deflection of the filament is elastic until the stress reaches a yield value, after which further deflection is plastic in nature, and produces a "permanent set" of the

beam. If the deflection is maintained over a period of time, creep will occur, and the stress in the beam will reduce. If the beam is in the elastic region, this creep is recovered when the beam is unloaded (although this may take some time). If the beam has yielded, then the stress reduction is associated with further permanent set.

In the elastic region, comparison of values of Young's Modulus, E, determined from the experiments in Chapter 4 and Appendix A show no consistent variation of E with time, and therefore we will regard E as a constant property of the material. This conflicts with the results in Figures 5.4 and 5.5 in Chapter 5, which show substantial relaxation of the bagasse compaction pressure when it is held at constant volume; relaxation which takes place over a time less than one second. The conflict may be seen as an inadequacy of the single filament experiments, and it is likely to be significant when calculating effects such as nipforces as the bagasse passes through a roller pair. However, for the present work, where we are interested in understanding the permanent set which arises from yield, which is thought to be the mechanism which makes compaction possible, the discrepancy is not considered to be significant.

For creep in the plastic region, Figure 4.2 suggests that the proportional creep rate is similar to that in the elastic region. Therefore, for a deflected beam, the amount of deflection which will subsequently appear as permanent set, σ , is given by

$$d\sigma/dt = k\delta ,$$

where δ is the total deflection of the beam, t is time, and k is a constant which, from the experiments, is given a value of 0.04. If it is assumed that σ is small compared with δ , then this can be integrated to yield

$$\sigma = 0.04\,\delta t . \qquad (1)$$

This permanent set should be added to that due to the initial, time independent, yield of the beam.

These concepts will subsequently be used to develop a model for the behaviour of bagasse when it is compacted. However, it should be remembered that considerable experimental inaccuracies were tolerated in the experiments of Chapter 4 and Appendix A, in order to allow formulation of a preliminary set of physical concepts. Whilst this is acceptable for present purposes, further experimental work would be needed in order to establish an accurate description of single filament behaviour.

7.2 A BAGASSE COMPACTION MODEL

MODELLING THE BAGASSE SAMPLE

The possibility of differing deflections amongst the bagasse filaments in a compaction sample would seem to make extrapolation from single filament properties to overall sample behaviour an impractical task. However, it can be tackled by following an approach suggested by the application of Statistical Mechanics to thermodynamic systems consisting of many small subsystems (Sears, 1980) - for example, the molecules of a gas, or the atoms in the matrix of a metal crystal.

Following Loughran (1981) the bagasse sample is modelled as a collection of many small beams, of varying length and cross section, which interact with each other through the forces and reactions occurring at the points of contact between the beams. Deflection of each beam requires it to store strain energy, and the task of determining the proportion of the total number of beams which have a given deflection is essentially that of determining the proportion which have stored the associated amount of strain energy.

In considering this problem, the spirit of the Van Wyck model, outlined by Loughran (1981), is followed. It is assumed that the collective behaviour of the beams can be represented

by considering a sample consisting of beams of one representative set of dimensions i.e. all the beams in the sample are identical. It is further assumed that each beam is loaded at midspan and, because each of the beams will be part of a bagasse filament consisting of many beams, the beams will deflect as if their ends were encastered. Thus the force, F_δ, associated with a deflection δ is given by Marks (1951).

$$F_\delta = 24(EI/b^3)\,\delta \qquad (1)$$

and the associated strain energy is

$$u = 12(EI/b^3)\,\delta^2 \qquad (2)$$

where b is the semispan of the beam, and I the second moment of area of the cross section.

MICROSTATES AND MACROSTATES

The state of a bagasse sample under a given degree of compression can be specified by specifying the strain energy of each individual beam in the sample. This is referred to as the specification of a "microstate". However, in considering the overall behaviour of the sample, interest is not centred on the level of strain energy of each individual beam, but rather, on determination of the number of beams which have a particular level of strain energy.
i.e. on determination of the distribution numbers N_1, N_2, N_3.....etc, where

N_1 beams have strain energy u_1
N_2 " " " " u_2
N_3 " " " " u_3
.....etc

This is referred to as specification of a "macrostate". It is clear that many differing microstates can correspond to any one particular macrostate.

It will also be noted that fixing the total amount of strain energy in a sample does not fix the distribution numbers - i.e. there are many possible macrostates corresponding to a given state of compression of the sample. The

task here is to determine which of these macrostates will apply in practice.

THE MOST PROBABLE MACROSTATE

The task is tackled by determining which of the macrostates has the maximum probability of occurrence. At first sight this may seem to leave an element of uncertainty regarding the state which may actually occur in a sample. In fact, for the very large numbers of beams involved in a typical sample, analysis shows that the probability of the most probable macrostate is many orders of magnitude higher than the combined probability of all possible macrostates and therefore that, for all practical purposes, the probability of occurence of the most probable macrostate is unity i.e. it is a certainty.

Now, there is no apparent mechanism which seems to favour the occurrence of any one possible microstate over any other, and therefore it is reasonable to assume that all microstates are equally probable. With this assumption, the probability of a given macrostate is W/W_o, where W is the number of possible microstates corresponding to that macrostate, and W_o is the total number of possible microstates. The most probable macrostate is that for which W/W_o is a maximum but, in order to simplify the following analysis, it will be noted that $\ln(W/W_o)$ is a maximum when W/W_o is a maximum, and the condition for a maximum in $\ln(W/W_o)$ will be sought.

Remembering that W is a function of the distribution numbers N_1, N_2 .....etc, then the condition for $\ln(W/W_o)$ to be a maximum as the N's are varied is that

$$\left\{\frac{\delta}{\delta N_1}(\ln W)\right\} dN_1 + \left\{\frac{\delta}{\delta N_2}\ln W)\right\} dN_2 + \ldots\ldots\ldots \text{etc} = 0, \qquad (3)$$

where $dN_1, dN_2, \ldots\ldots$etc are small variations in $N_1, N_2, \ldots\ldots$etc.

This is subject to two further conditions. The first is that equ 5.2 (Loughran 1981) shows that at a given overall volume (i.e. a given degree of compression of the sample) the total

number of beams within the sample is fixed. Therefore, the N's can only be varied according to the condition

$$dN_1 + dN_2 + \ldots\ldots\ldots\ldots = 0 \qquad (4)$$

The second is that the total strain energy must remain constant

$$\text{i.e.} \quad u_1\, dN_1 + u_2\, dN_2 + \ldots\ldots\ldots\ldots = 0 \qquad (5)$$

These three equations can be combined into one by using Lagranges "Method of Undetermined Multipliers"
i.e. equ (4) is multiplied by a , and equ (5) by 6 , where a and B are constants which are chosen such that

$$\frac{\delta}{\delta N_1}(\ln W) + \alpha + \beta u_1 = 0$$

and $$\frac{\delta}{\delta N}(\ln W) + \alpha + \beta u_2 = 0.$$

When the resulting equs (4) and (5) are added to equ (3), there results

$$\{\frac{\delta}{\delta N_1}(\ln W) + \alpha + \beta u_1\}\, dN_1 + \{\frac{\delta}{\delta N_2}(\ln W) + \alpha + \beta u_2\}\, dN_2 + \ldots = 0$$

The dN's in this equation can be varied independently, implying that the coefficients must be zero and therefore that, for the most probable macrostate

$$\frac{\delta}{\delta N_i}(\ln W) + \alpha + \beta u_i = 0, \qquad (7)$$

where i = 1, 2, 3, ...etc.

Now, if there are N beam elements in the sample, the number of microstates corresponding to the macrostate specified by the distribution numbers N_1 , N_2 , ...etc. is simply the number of ways N elements can be organized into groups of N_1 , N_2 , ...etc. This is derived in Appendix B, and leads to the result that

$$W = \frac{N!}{N_1!\, N_2!\, N_3!} \ldots\ldots\ldots \qquad (8)$$

Substituting this in equ (7) yields

$$-\frac{\delta}{\delta N}(\ln N_i!) + \alpha + \beta u_i = 0,$$

since N is a constant. If Stirling's approximation is now used in the form

$$\ln N_i! = N_i \ln N_i - N_i,$$

(where N_i is taken to be a large number), then

$$\frac{\delta}{\delta N_i}(\ln N_i!) = \ln N_i,$$

whence

$$-\ln N_i + \alpha + \beta u_i = 0$$

or

$$N_i = \exp\alpha \exp(\beta u)$$

Remembering that $\sum_i N_i = N$, then this relation can be written as

$$N_i = (N/Z) \exp(\beta u_i), \qquad (9)$$

where $Z = \sum_i \exp(\beta u_i)$.

CONTINUOUSLY VARYING STRAIN ENERGY,

So far, it has been assumed that the strain energy in the beams takes up discrete energy levels u_1, u_2, ...etc. However, equ (9) can readily be interpreted for the case where the allowable energy levels vary in a continuous manner (as in the practical case) by rewriting it in the form

$$dN_\delta = (N/Z) \exp(\beta u), \qquad (10)$$

where dN_δ is the number of beams with deflection between δ and $\delta + d\delta$, and Z is written as

$$Z = h^{-1} \int_0^\infty \exp(\beta u)\, d\delta, \qquad (11)$$

where the summation for Z has been changed to an integral by dividing the continuous variation of δ into small equal intervals of magnitude h.

To obtain β, it is noted that the total strain energy of the sample, U, is given by

$$U = h^{-1} \int_0^\infty u \, dN_\delta \, d\delta$$

Incorporating equ(10) into this relation, substituting for u from equ(2) and remembering the standard integrals

$$\int_0^\infty \exp(-ax^2)\, dx = 0.5 \sqrt{\pi/a} ,$$

$$\int_0^\infty \exp(-ax)\, x\, dx = 0.25\, a^{-1} \sqrt{\pi/a} ,$$

it is found that $\beta = -N/2U$, whence

$$Z = h^{-1} \frac{\sqrt{\pi}}{2} \sqrt{\frac{N}{2U}} \frac{12EI}{b^3} \qquad (12)$$

and

$$dN_\delta = \frac{2}{\sqrt{\pi}} Nh \sqrt{\frac{N}{2U}} \frac{12EI}{b^3} \exp(-0.5uN/U). \qquad (13)$$

Thus, although the fraction of the beams with strain energy u decreases exponentially as u increases with respect to the average energy per beam, nevertheless there is, in principle, always some beams with strain energy greater than any given value. This implies there will always be some beams with deflection much greater than the average.

AVERAGE DEFLECTION AND PERMANENT SET

The average deflection of the beams in the sample is given by

$$\delta_m = N^{-1} h^{-1} \int_0^\infty \delta \, dN_\delta \, d\delta ,$$

which, substituting from equs(13) and (2), and performing the integration, can be written as

$$\delta_m = \left(\sqrt{\frac{\pi N}{2U}} \frac{12EI}{b^3} \right)^{-1} \qquad (14)$$

The permanent set arises from plastic yield associated with the initial state of compression of the sample, when some beam elements are deflected beyond their yield point, and from the plastic creep which subsequently occurs in those beam elements.

Considering first the initial yield, the average permanent set resulting from this is given by

$$\sigma_{1Y} = N^{-1} h^{-1} \int_{\delta_Y}^{\infty} (\delta - \delta_Y)\, dN_\delta\, d\delta \qquad (15)$$

where δ_Y is the deflection at which a beam begins to yield.
To evaluate this equation, equs(13) and (2) are used to substitute for dN_δ. The use of equ(2) is strictly not justified when beam deflections exceed δ_Y, as the elastic relationship between strain energy and deflection no longer applies. However, it will serve as a reasonable approximation for beam deflections which are not too much in excess of δ_Y, and since equ(13) shows that this is likely to include the majority of the beams undergoing plastic deformation, it is considered that the error involved in using equ(2) is acceptable because of the convenience it offers. Making these substitutions, and employing equ(14), equ(15) becomes

$$\sigma_{1Y} = 2\,(\pi\delta_m)^{-1} \int_{\delta_Y}^{\infty} (\delta - \delta_Y) \exp(-\delta^2/\pi\delta_m^2)\, d\delta.$$

This can be evaluated approximately by writing

$$\delta^2 = (\delta - \delta_Y)^2 + 2(\delta - \delta_Y)\,\delta_Y + \delta_Y^2,$$

whence

$$\sigma_{1Y} = \frac{2}{\pi\delta_m} \exp\left(\frac{-\delta_Y^2}{\pi\delta_m^2}\right) \int_0^{\infty} \exp\left(\frac{-(\delta-\delta_Y)^2}{\pi\delta_m^2}\right) \exp\left(\frac{-2\delta_Y(\delta-\delta_Y)}{\pi\delta_m^2}\right)(\delta-\delta_Y)\,d(\delta-\delta_Y)$$

Integrating by parts, this becomes

$$\sigma_{1Y} = \left\{\delta_m - \frac{2\delta_Y}{\pi\delta_m} \int_0^{\infty} \exp\left(\frac{-(\delta-\delta_Y)^2}{\pi\delta_m^2}\right) \exp\left(\frac{-2\delta_Y(\delta-\delta_Y)}{\pi\delta_m^2}\right) d(\delta-\delta_Y)\right\} \exp\frac{-\delta_Y^2}{\pi\delta_m^2}.$$

Now, for $\delta_Y/\delta_m >> 1$, the last term ensures that $\sigma_{1Y} \to 0$, implying that no permanent set is associated with small mean deflections.

For larger values of δ_m, the second exponential term in the integrand of the integral within the brackets can be written as

$$\exp\left(\frac{-2\delta_Y(\delta-\delta_Y)}{\pi\delta_m^2}\right) \quad = \quad 1- \quad \frac{2\delta_Y(\delta-\delta_Y)}{\pi\delta_m^2} \quad ,$$

when $(\delta - \delta_Y)\ \delta_m << 1$, whilst the first exponential term ensures that, for larger values of $(\delta - \delta_Y)/\delta_m$, no significant contribution is made to the integral. With this substitution, the integral can be evaluated to yield

$$\sigma_{IY} = \delta_m \left\{1 - \frac{\delta_Y}{\delta_m} + \frac{2}{\pi}\left(\frac{\delta_Y}{\delta_m}\right)^2\right\} \exp\left(-\frac{\delta_Y^2}{\pi\delta_m^2}\right) \quad (16)$$

Equ(16) is plotted in Figure 7.1. It can be seen that no significant initial yield occurs until the average deflection approaches roughly 30% of the yield deflection. Further increase in average deflection then rapidly increases the permanent set due to yield to nearly half of the average defection, after which it constitutes a slowly increasing fraction of the average deflection.

The second part of the permanent set, due to plastic creep, can be written as

$$\sigma_{2Y} = N^{-1}\, h^{-1} \int_{\delta_Y}^{\infty} 0.04\ \delta t\ dN_\delta\ d\delta,$$

where equ(1), from §7.1, has been used for the creep of the individual beam elements. Using equs(13), (2) and (14), this can be integrated to yield

$$\sigma_{2Y} = \delta_m \left\{0.04\ \exp\left(-\delta_Y^2/\pi\delta_m^2\right)\right\}\ t\ . \quad (17)$$

BULK COMPACTION PROPERTIES

The final density of a compacted bagasse pellet, after the compaction process is completed, depends upon the permanent set which is induced within the fibres of the pellet. This is compounded of the permanent set due to initial yield, and that due to retention (identified here as plastic creep). Here we concentrate on the first.

The permanent set due to initial yield can be deduced from equ(16). The mean deflection of the beams is proportional to the movement of the boundaries of a pellet as it is compressed. Thus, if the pellet is being formed in a cylinder, the deflection at peak compression, δ_{mp}, will be proportional to the movement of the piston i.e.

$$\delta_{mp} \propto (v_i - v_p)$$

or

$$\delta_{mp} = K (\rho_i^{-1} - \rho_p^{-1})$$

where v_i and ρ_i are the initial volume and density, v_p and ρ_p are the respective values at peak compression, and K is a constant which includes the mass of the pellet. When the compression pressure is released, without retention, the pellet density falls to a value ρ_s, associated with the beam elements of the sample reducing their deflection from

$$\delta_{mp} \text{ to } (\delta_{mp} - \sigma_{1Yp}), \quad \text{and therefore}$$

$$\delta_{mp} - \sigma_{1Yp} = K (\rho_s^{-1} - \rho_p^{-1}).$$

thus

$$\sigma_{1Yp} = K (\rho_i^{-1} - \rho_s^{-1})$$

or

$$\sigma_{1Yp}/\delta_{mp} = (\rho_i^{-1} - \rho_s^{-1})/(\rho_i^{-1} - \rho_p^{-1}). \quad (18)$$

Now, to determine the value of σ_{1Yp}/δ_{mp} from equ(16) requires that the value of δ_Y/δ_{mp} be known. For a beam with fixed ends, a span 2b, and a circular cross section of diameter d, which is loaded at the midspan, the relation between yield stress and deflection is given by

$$\delta_Y = f_Y \, b^2/3 \, dE,$$

whence, using equ(14), noting that $N = \ell/2b^{(2)}$, and that

$$\pi \ell \, d^2 = 4m/\rho_f,$$

where ℓ is the total fibre length within the pellet, ρ_f is the fibre density, and ρ_p the peak charge density, it follows that

$$\frac{\delta_Y}{\delta_m} = \sqrt{\frac{\ell}{48}\frac{\rho_p}{\rho_f}\frac{1}{U'E}}\, f_Y \quad , \qquad (19)$$

where U' is the strain energy per unit volume. This may be obtained from the relation

$$U' = 14\ \rho_p\ (\rho_p/1100)^2 \ \text{kJ/m}^3 \ , \qquad (20)$$

which has been chosen to fit the experimental results at 10% moisture in Table 6.1 of Chapter 6. With f_Y = 100 MPa., ρ_f = 800 kg/m , and E = 10^5 MPa n or 5×10^5 MPa, equ(19) leads to the following values for δ_Y/δ_{mp}.

TABLE 7.1 YIELD AT PEAK COMPRESSION

ρ_p (kg/m^3)		1100	800	600	400
$\frac{\delta_Y}{\delta_{mp}}$	E = 5 x 10^5 MPa	.11	.15	.20	.30
	E = 10^5 MPa	.25	.34	.45	.67

When these results are translated into abscissa on Figure 7.1, it is seen that the pellet is well into the region where initial permanent set takes place at all significant peak compaction densities.

In order to employ equ(18) to compare predictions with experimental results, a suitable value of ρ_i must be chosen. This must correspond to a point in the compaction process where fibres begin to deflect as beams i.e. significant forces begin to be generated. Figure 3.10-1 (Anderson 1983) shows that this occurs for ρ_i = 250 kg/m. Using these values, Figure 7.2 is used to compare equ(18) with experimental results from Figure 3.5-1 (Anderson 1983). It can be seen that the

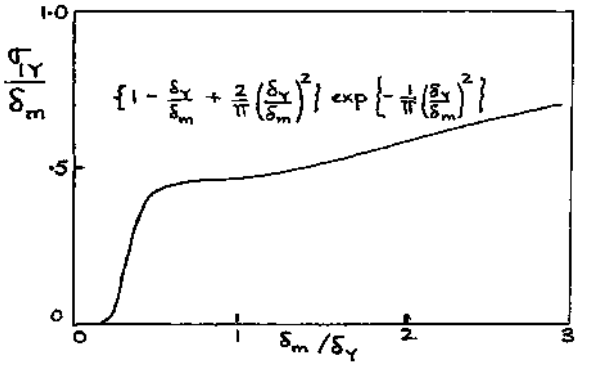

FIGURE 7.1 EFFECT OF MEAN DEFLECTION ON PERMANENT SET

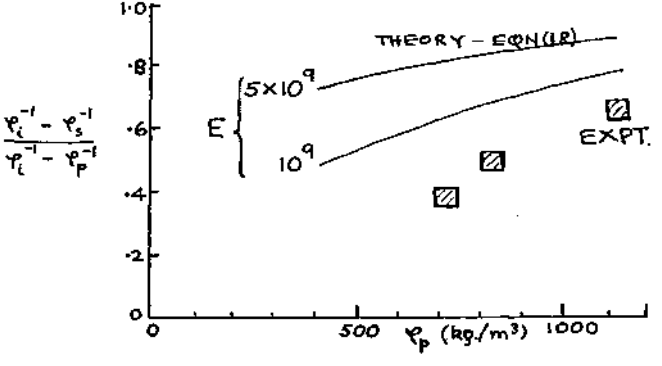

FIGURE 7.2 INITIAL PERMANENT SET - THEORY VS EXPERIMENT

permanent set is over-predicted by the theory, although discrepancies could well be associated with uncertainties in the basic data. However, the fact that experiment and theory are not too widely separated at this stage is very encouraging.

CHAPTER 8
FRICTION TESTS

8-1 AIM

To determine the coefficients of shear and/or friction for bagasse pellets on different surfaces at various temperatures, pressures and moisture contents, so that this information may be used in the development of the bagasse pelleting machine at Sugar Research Institute.

The surfaces investigated were:

i) smooth mild steel (MS)
ii) smooth cast iron (CS)
iii) grooved cast iron (CG)
(triangular grooves; depth 3 mm, pitch 5 mm)

The surface finish on the plates was initially 50um in the direction of slip but this finish was subject to very rapid wear which reduced the roughness significantly after two or three tests at 35 MPa pellet pressure. While it was relatively easy to reroughen the smooth plates with some coarse emery cloth, it was found to be quite time consuming attempting the same task on the grooved plate, where grinding powder and a grooved block were employed. In addition, it was very difficult to ensure that the surfaces of the plates were completely free of residue from the roughening process.

Therefore it was decided that all tests would be conducted at the "equilibrium" roughness for each plate and that the only surface preparation of the plates would be to use a scraper to remove any bagasse adhering to them.

8.2 APPARATUS

The experimental rig consisted of three hydraulic cylinders arranged on a support structure. The two horizontal

cylinders were used to press the pellets onto each side of a friction plate. The vertical cylinder was used to push the plate between the pellets. A displacement transducer mounted on the cylinder and attached to the end of the ram was used to provide the location and hence velocity of the friction plate during each test. The oil pressure in the cylinders was measured with pressure transducers. The pressures and displacement were recorded as function of time on an electrostatic chart recorder.

8.3 METHOD

Pellets of the suitable density and thickness were formed on the INSTRON. They were stored until required in sealed plastic bags so that moisture loss would be minimal.

Pellets for the 80°C and 140°C tests were formed in a 69.8 mm diameter cylinder so that two pellets could be pushed into each of the standard 76.2 mm diameter cylinders which were sealed and placed in the oven for heating to the test temperature. An experiment had been conducted to determine the time required for this (Figure 8.1).

The force to be applied to the pellets was set to the required value by adjusting the relief valve on the 3-way valve which was used to control the movement of the horizontal rams. Because the air supply pressure varied considerably/ this was found to be a more reliable way of producing the desired force than attempting to regulate the air supply to the pneumatically powered hydraulic pump which drove the rams.

Once the relief valve had been set the rams were positioned for the test and the friction plate propped into place with a piece of wood. The pellets were placed between the plattens on the rams and the friction plate and loaded to the set force.

In the 80°C and 140°C tests, the friction plate and plattens were heated in the oven in order to simulate as closely as possible the conditions being modelled and reduce cooling of the pellets.

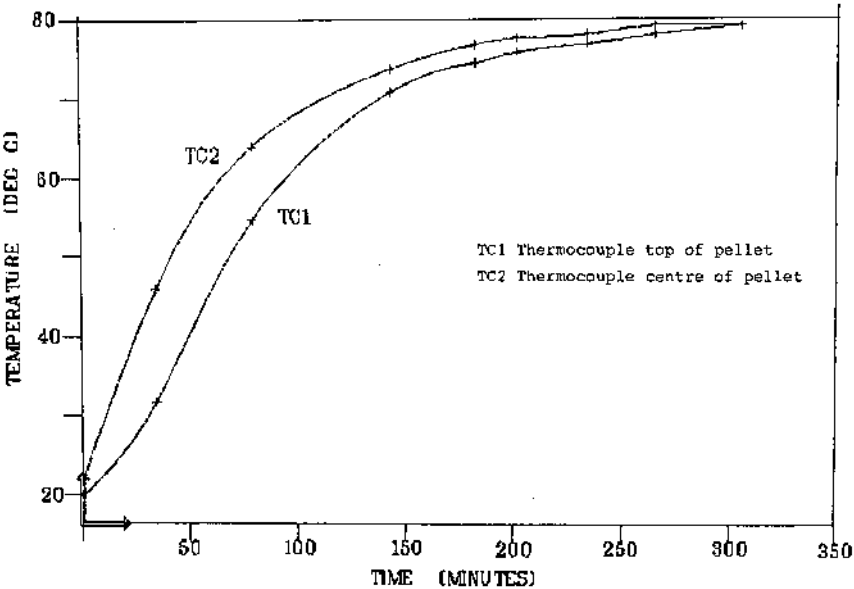

FIGURE 8.1 RELATIONSHIP BETWEEN PELLET TEMPERATURE AND TIME

Next, the piece of wood supporting the friction plate was removed and the alignment of the friction plate checked to ensure that it would not foul on the pellet supports as it was pushed between the pellets.

At this stage the procedure adopted depended on the force applied to the pellets.

i) High Pressure

At the two high values corresponding to 35 and 10 MPa pellet pressure it was possible to drive the vertical ram down at low pressure until it stopped at the friction plate. This preloaded the structure and reduced the movement produced by the next stage which was the application of full pressure to the cylinder.

ii) Low Pressure

At the lowest pellet pressure (1 MPa) it was found that the force produced by the vertical cylinder was sufficient to cause slow movement of the friction plate and thus preloading could not be achieved. Fortunately very little movement of the structure occurred during tests and so this posed no problems.

Immediately before full pressure was applied to the vertical cylinder, the chart drive was switched on.

During all tests, careful attention was given to the progress and alignment of the friction plate so that, at the first indication of trouble, the ram's direction could be reversed and the plate stopped before severe damage occurred.

The maximum travel of the friction plate was 285 mm or approximately 3.6 pellet diameters.

8.4 RESULTS

It was observed that shear of the bagasse fibres in the pellets occurred in some cases, particularly at high pressure. These instances are marked with an asterisk in the tables of results.

8.4.1 RESULTS FOR COEFFICIENT OF STATIC FRICTION AT 20°C

The results of the tests conducted on whole material at 20°C for a range of surfaces, moisture contents and pressures, are outlined in Table 8.1 and the results of the analysis of variance are shown in Table 8.2. It can be seen that all of the factors investigated significantly influenced the coefficient of static friction and that all interactions were significant.

TABLE 8.1. COEFFICIENT OF STATIC FRICTION

		Friction Plate					
		Mild Steel		Cast Iron			
Moisture Content %	Pressure MPa	Smooth (F_1)		Smooth (F_2)		Grooved (F_3)	
		R_1	R_2	R_1	R_2	R_1	R_2
10 (W_1)	35 (P_1)	.39*	.33*	.37*	.37*	.42*	.40*
	10 (P_2)	.35	.29	.34	.34	.48*	.49*
	1 (P_3)	.13	.12	.23	.16	.38	.30
20 (W_2)	35	.44	.39	.40	.41	.71*	.76*
	10	.28	.31	.35	.39	.54*	.53*
	1	.31	.35	.31	.33	.43	.40
30 (W_3)	35	.14	.14	.14	.14	.30	.29
	10	.27	.28	.27	.25	.39	.36
	1	.35	.38	.30	.27	.29	.31

Figures 8.2 to 8.7 illustrate the significant single factor effects and interactions.

Single Factor Effects

It can be seen that, averaged over all other variables, the coefficient of static pressure increases with applied pressure from 1 to 10 MPa with no increase from 10 to 35 MPa. The coefficient of static friction is seen to be maximum at 20 per cent moisture and whilst, as expected, the coefficient is highest with grooved surfaces, there is no difference in the coefficient of friction between the mild steel and cast iron surfaces.

Interactions

Perhaps the most interesting of the interactions is the more rapid fall off in the coefficient of static friction at the highest pressure as the moisture content of material increases.

TABLE 8.2. RESULTS OF ANALYSIS OF VARIANCE OF RESULTS CARRIED OUT AT 20°C.

Source	Degrees of Freedom	Variance Ratio	Significance Level
F	2	167.142	< .001
W	2	166.926	< .001
P	2	39.235	< .001
FW	4	14.229	< .001
FP	4	7.596	< .001
WP	4	71.684	< .001
FWP	8	11.705	< .001
ERROR	27		
TOTAL	53		

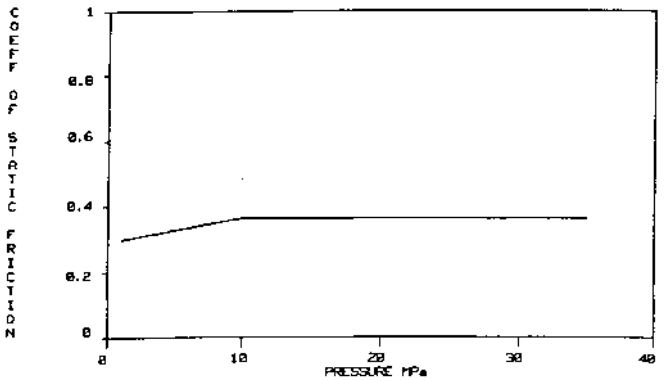

FIGURE 8.2 INFLUENCE OF APPLIED PRESSURE ON COEFFICIENT OF STATIC FRICTION.

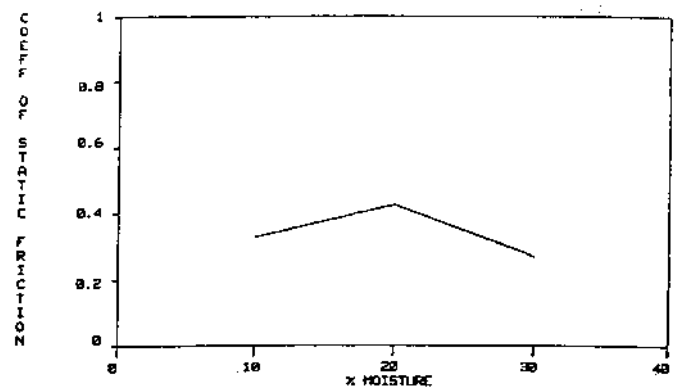

FIGURE 8,3 INFLUENCE OF MOISTURE CONTENT ON COEFFICIENT OF STATIC PRESSURE.

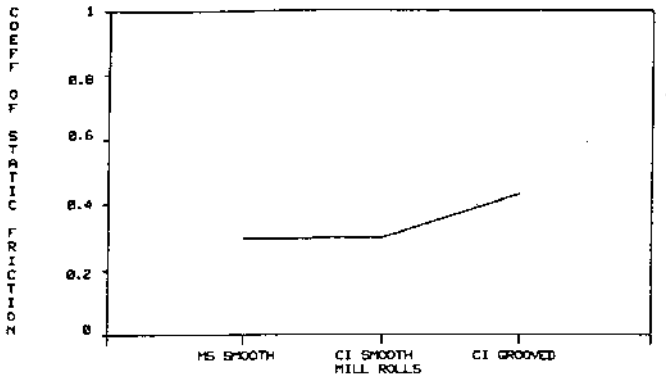

FIGURE 8.4 INFLUENCE OF SURFACE ON COEFFICIENT OF STATIC FRICTION.

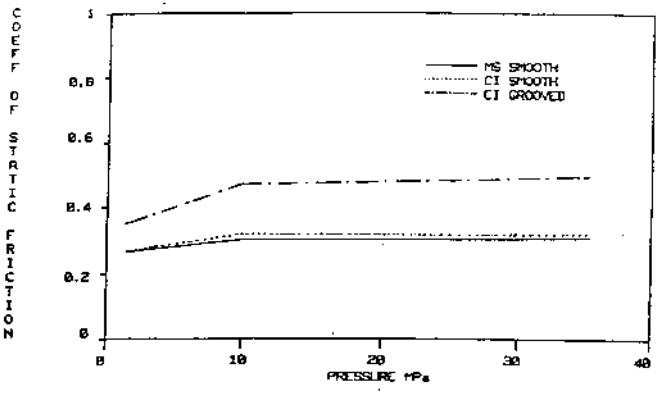

FIGURE 8.5 ILLUSTRATION OF SURFACE PRESSURE INTERACTION.

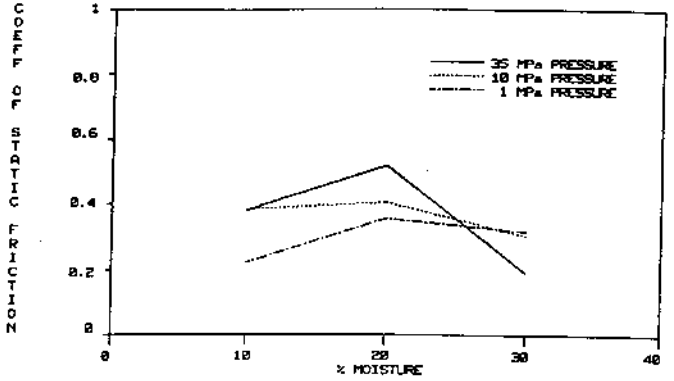

FIGURE 8.6 ILLUSTRATION OF PRESSURE MOISTURE INTERACTION.

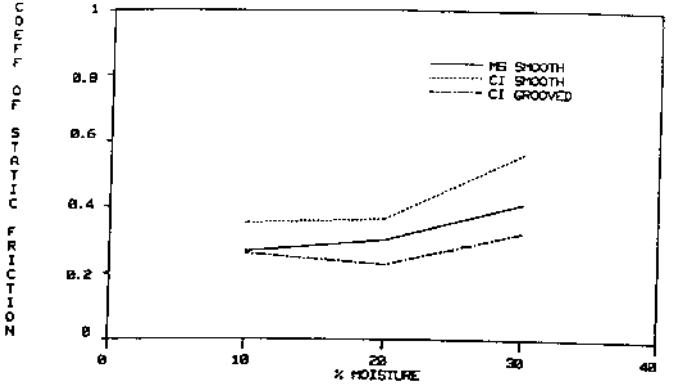

FIGURE 8.7 ILLUSTRATION OF SURFACE, MOISTURE INTERACTION,

8.4.2 RESULTS OF COEFFICIENT OF STATIC FRICTION TESTS WITH DIFFERENT MATERIAL SIZE - 20°C

A series of tests was carried out at 10 per cent moisture with both coarse and whole material to investigate the influence of material size for a range of pressures and surfaces. The results obtained are shown in Table 8.3 and the results of the analysis of variance are shown in Table 8.4. From this it can be seen that only the single factors were significant and there were no significant interactions.

TABLE 8.3. COEFFICIENT OF STATIC FRICTION FOR DIFFERENT MATERIAL SIZE - TEMPERATURE 20°C, MOISTURE 10%.

		Friction Plate					
		Mild Steel		Cast Iron			
Material Size	Pressure MPa	Smooth (F_1)		Smooth (F_2)		Grooved (F_3)	
		R_1	R_2	R_1	R_2	R_1	R_2
Whole (M_1)	35 (P_1)	.39*	.33*	.37*	.37*	.42*	.40*
	10 (P_2)	.35	.29	.34	.34	.48*	.49*
	1 (P_3)	.13	.12	.23	.16	.38	.30
Coarse (M_2)	35	.22*	.28*	.25*	.28*	.34*	.38*
	10	.26*	.23*	.30*	.28*	.38*	.35*
	1	.16	.14	.13	.13	.21	.27

The influences of pressure and material are similar to those illustrated in Figures 8.2 and 8.4. Figure 8.8 illustrates that the coefficient of static friction is marginally less with the coarser material.

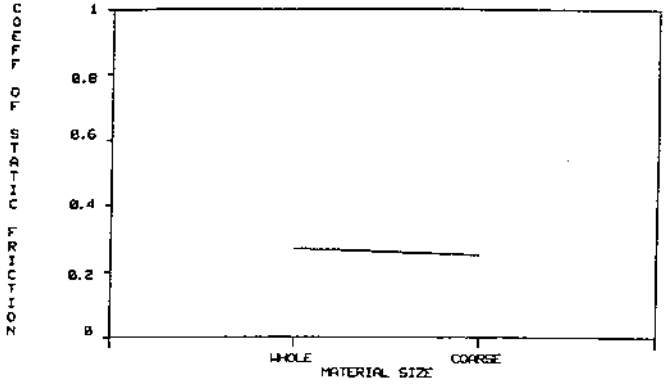

FIGURE 8.8 INFLUENCE OF MATERIAL SIZE ON COEFFICIENT OF STATIC FRICTION.

TABLE 8.4. RESULTS OF ANALYSES OF VARIANCE OF RESULTS FOR DIFFERENT MATERIAL SIZE.

Source	Degrees of Freedom	Variance Ratio	Significance Level
F	2	61.191	< .001
M	1	59.247	< .001
P	2	95.295	< .001
FM	2	1.568	.100 - .250
FP	4	2.595	.050 - .100
MP	2	2.130	.100 - .250
FMP	4	2.846	.050 - .100
ERROR	18		
TOTAL	35		

TABLE 8.5. COEFFICIENT OF DYNAMIC FRICTION
MATERIAL: WHOLE, 20°C

		Friction Plate					
		Mild Steel		Cast Iron			
Moisture Content %	Pressure MPa	Smooth (F_1)		Smooth (F_2)		Grooved (F_3)	
		R_1	R_2	R_1	R_2	R_1	R_2
10 (W_1)	35 (P_1)	.38*	.33*	.37*	.39*	.48*	.35*
	10 (P_2)	.35	.29	.36	.34	.48*	.54*
	1 (P_3)	.13	.12	.23	.16	.37	.30
20 (W_2)	35	.36	.35	.35	.35	.62*	.61*
	10	.25	.33	.35	.39	.52*	.46*
	1	.31	.35	.31	.33	.43	.40
30 (W_3)	35	.25	.28	.35	.31	.52	.48
	10	.26	.23	.30	.28	.38	.35
	1	.14	.16	.13	.13	.27	.21

TABLE 8.6. RESULTS OF ANALYSIS OF VARIANCE OF RESULTS FOR COEFFICIENT OF DYNAMIC FRICTION - COARSE MATERIAL, 20°C.

Source	Degrees of Freedom	Variance Ratio	Significance Level
F	2	114.025	< .001
W	2	50.256	< .001
P	2	91.510	< .001
FW	4	0.962	
FP	4	1.536	.100 - .250
WP	4	8.984	< .001
FWP	3	5.126	< .001
ERROR	27		
TOTAL	53		

8.4.3 RESULTS FOR DYNAMIC COEFFICIENT OF FRICTION - 20°C

The results of the coefficient of dynamic friction for whole material at 20°C are summarised in Table 8.5 and the results of the analysis of variance of the results are shown in Table 8.6.

All factors investigated were significant and these effects are illustrated in Figures 8.9 to 8.11, which show similar trends to those exhibited for the coefficient of static friction.

8.4.4 RESULTS OF COEFFICIENT OF DYNAMIC FRICTION TESTS WITH DIFFERENT MATERIAL SIZE - 20°C.

The results obtained for tests on whole and coarse material are shown in Table 8.7. The results of the analysis of variance on the data is shown in Table 8.8. It is seen that the influence of material size is significant and similar to that found for the coefficient of static friction. This influence is illustrated in Figure 8.12.

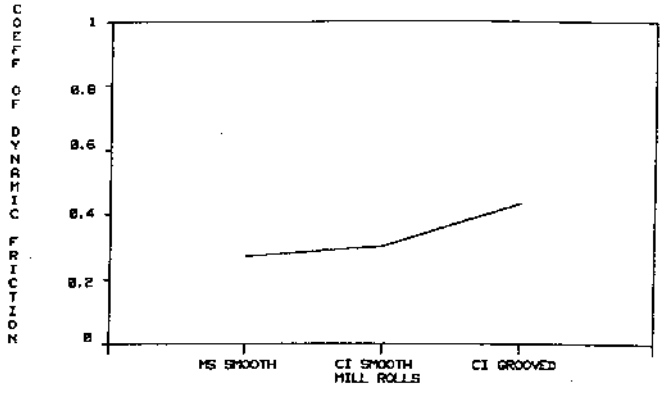

FIGURE 8,9 INFLUENCE OF SURFACE ON COEFFICIENT OF DYNAMIC FRICTION,

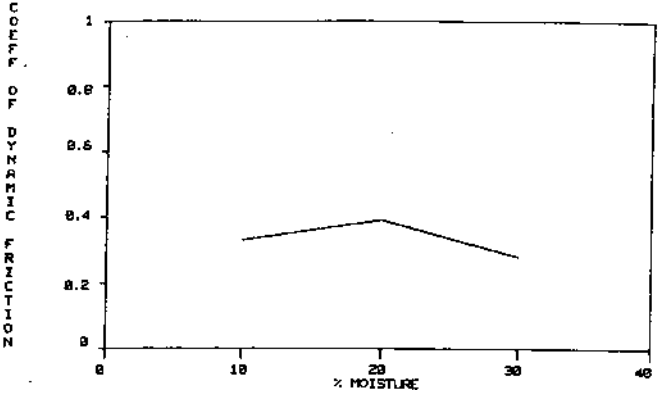

FIGURE 8.10 INFLUENCEOF MOISTURE ON COEFFICIENT OF DYNAMIC FRICTION

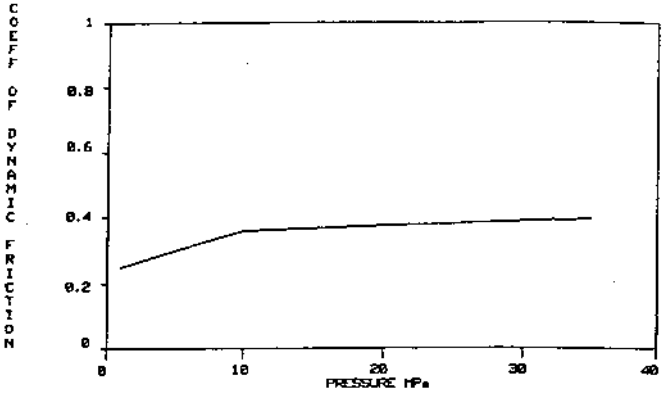

FIGURE 8.11 INFLUENCE OF PRESSURE ON COEFFICIENT OF DYNAMIC FRICTION,

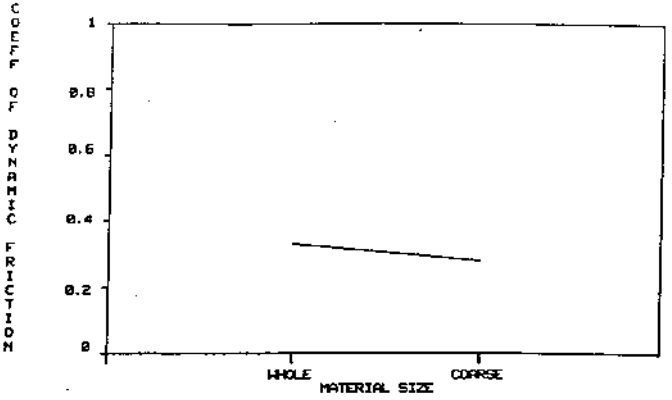

FIGURE 8.12 INFLUENCE OF MATERIAL SIZE ON COEFFICIENT OF DYNAMIC FRICTION.

TABLE 8.7. COEFFICIENT OF DYNAMIC FRICTION - TEMPERATURE 20°C, MOISTURE 20%.

		Friction Plate					
		Mild Steel		Cast Iron			
Material Size	Pressure MPa	Smooth (F_1)		Smooth (F_2)		Grooved (F_3)	
		R_1	R_2	R_1	R_2	R_1	R_2
Whole(M_1)	35 (P_1)	.38*	.33*	.37*	.39*	.48*	.35*
	10 (P_2)	.35	.29	.36	.34	.48*	.54*
	1 (P_3)	.13	.12	.23	.16	.37	.30
Coarse(M_2)	35	.25*	.28*	.35*	.31*	.52*	.48*
	10	.26	.23	.30	.28	.38*	.35*
	1	.16	.14	.13	.13	.21	.27

TABLE 8.8. RESULTS OF ANALYSIS OF VARIANCE OF TESTS TO DETERMINE EFFECT OF MATERIAL SIZE ON DYNAMIC COEFFICIENT OF FRICTION.

Source	Degrees of Freedom	Variance Ratio	Significance Level
F	2	56.393	< .001
M	1	18.587	< .001
P	2	83.714	< .001
FM	2	0.073	
FP	4	0.125	
MP	2	3.283	.050 – .100
FMP	4	5.393	.001 – .010
ERROR	18		
TOTAL	35		

8.4.5 INFLUENCE OF TEMPERATURE

A series of tests was carried out to determine the influence of temperature on the coefficient of friction. The tests were carried out on whole material at 10 per cent moisture for three levels of pressure on each of the three surfaces.

The results are shown in Table 8.9. The results of an analysis of variance carried out on these data are shown in Table 8.10. This shows that temperature had a significant effect on the coefficients of friction. Several tests were carried out at 140°C and the results are shown in Table 8.11. Figures 8.13 and 8. 14 show the extent to which the coefficients of friction decrease as temperature increases. It is interesting to note from Table 8.10 that there is no significant difference between the values of coefficient of static and dynamic friction.

TABLE 8.9. RESULTS OF COEFFICIENTS OF FRICTION AT 20°C AND 80°C MATERIAL - WHOLE, 10% MOISTURE.

Friction Type	Temp °C	Pressure MPa	Friction Plate: Mild Steel Smooth(F_1) R_1	Mild Steel Smooth(F_1) R_2	Cast Iron Smooth(F_2) R_1	Cast Iron Smooth(F_2) R_2	Cast Iron Grooved(F_3) R_1	Cast Iron Grooved(F_3) R_2
STATIC A_1	20 (T_1)	35 (P_1)	.39	.33	.37	.37	.42	.40
		10 (P_2)	.35	.29	.34	.34	.48	.49
		1 (P_3)	.13	.12	.23	.16	.38	.30
	80 (T_2)	35	.34	.30	.33	.25	.35	.39
		10	.17	.14	.12	.13	.41	.36
		1	.01	.01	.09	.10	.16	.15
DYNAMIC A_2	20 (T_1)	35	.38	.33	.37	.39	.48	.35
		10	.35	.29	.36	.34	.48	.54
		1	.13	.12	.23	.16	.37	.30
	80 (T_2)	35	.28	.27	.25	.25	.39	.39
		10	.17	.14	.17	.13	.41	.40
		1	.10	.10	.10	.10	.16	.15

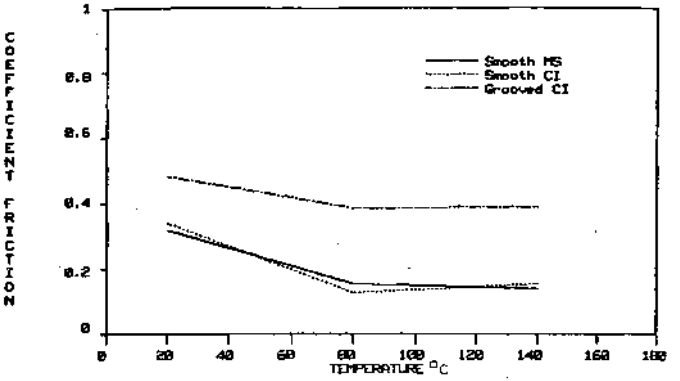

FIGURE 8,13 INFLUENCE OF TEMPERATURE ON COEFFICIENT OF STATIC FRICTION,

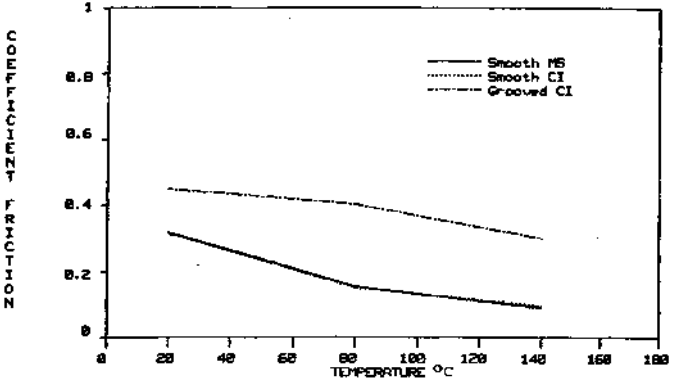

FIGURE 8.14 INFLUENCE OF TEMPERATURE ON COEFFICIENT OF DYNAMIC FRICTION,

TABLE 8.10. RESULTS OF ANALYSIS OF VARIANCE OF COEFFICIENTS OF FRICTION AT 20° AND 80°C.

Source	Degrees of Freedom	Variance Ratio	Significance Level
F	2	148.702	< .001
A	1	0.550	
T	1	233.250	< .001
P	2	230.031	< .001
FA	2	0.133	
FT	2	2.233	.100 ~ .250
FP	4	13.934	< .001
AT	1	0.022	
AP	2	1.325	> .250
IP	2	12.052	< .001
FAT	2	0.183	
FAP	4	1.255	> .250
FTP	4	6.346	< .001
ATP	2	1.490	.100 ~ .250
FATP	4	0.908	
ERROR	36		
TOTAL	71		

TABLE 8.11. COEFFICIENTS OF FRICTION AT 140°C - MATERIALS: WHOLE, 10% MOISTURE. PRESSURE 10 MPa.

	Friction Plate			
	Mild Steel	Cast Iron		
	Smooth	Smooth		Grooved
Static	.14	.14	.17	.39
Dynamic	.09	.09	.10	.30

8.5 CONCLUSIONS

The results outlined in this chapter have illustrated the following major factors affecting the coefficient of friction of relatively dry bagasse.

Very high values of coefficient of friction can be obtained. The highest values of greater than .7 for static friction occur with grooved surfaces at 20 per cent moisture.

The coefficient of static and dynamic friction increase with pressure except at the 30 per cent moisture level where expression of moisture at the higher pressures causes the coefficient of friction to decrease.

There was little difference between values obtained for flat cast iron and steel surfaces. As expected the coefficient of friction increased for grooved surfaces compared to flat surfaces.

Coarse material had lower coefficient of friction than whole material.

Whilst the coefficient of dynamic friction was somewhat less than the coefficient of static friction when the values were high on average there was no significant difference between the two coefficients over the range of tests.

The coefficient of friction decreased as temperature increased in the range 20°C to 140°C.

REFERENCES

Sears, F.W. "An Introduction to Thermodynamics, The Kinetic Theory of Gases, and Statistical Mechanics". Addiston-Wesley, U.S.A. 2nd Edition, June 1980.

Loughran, J.G. "Some Aspects of the Mechanics of Bagasse Compaction" M.Eng.Sc. Thesis, Department of Mechanical Engineering, University of Queensland, 1981.

Marks, L.S. "Mechanical Engineers' Handbook" 5th Edition, McGraw-Hill Book Coy. Inc., 1951.

Anderson, C.N., et al. Final Report "Elimination of Fuel Oil for Steam Generation in the Sugar Industry" Part 2, University of Queensland component. Department of Mechanical Engineering Research Report 3/83.

APPENDIX A

RAPID BENDING OF BAGASSE FIBRE BUNDLES

INTRODUCTION

This rapid fall off of load on the bagasse pellets which was observed during the compression tests conducted on the Instron materials testing machine in the Department of Mechanical Engineering (see Figures 5.4 and 5.5) indicated that the relaxation processes which governed the formation of a good quality pellet occurred in the order of 0.4 s or less.

In order to gain some further understanding of the relaxation process it was decided to investigate the response of some typical or average fibre bundles to loads of the order of those required to cause failure of the bundle.

PROCEDURE

The apparatus used is shown schematically in Figure A.1. The fibre bundle was placed across two smooth metal supports 12.5 ± 0.05 mm apart. A chosen mass was placed on the hinged support and the height of the hook adjusted until it was in contact with, but not visibly deforming, the fibre bundle.

A black wooden dowel with a white line on it was placed beside the mass. This provided a time reference for the experiment as its motion was that due to gravity only. The time reference was necessary because there was a ± 1.5 ms variation in the time required for the relay to release the hinged support.

Once the fibre bundle, mass and dowel had been placed in position and the camera focused and loaded, the test began. The electronic timing apparatus was triggered by opening the shutter. This immediately provided the 12 V required to open the relay and started the counter which provided the delay for

the triggering of the stroboscope. The delay and time interval between flashes could be varied in increments of 2.5, 5 or 10 ms. The number of flashes could be varied between 1 and 10.

Satisfactory photographs were obtained with delays of 12.5 and 15 ms and intervals between flashes of 10 and 20 ms. The shutter was held open for 1/8 s (nominally 125 ms). A typical photograph is reproduced in Figure A.2.

The separation of the images of the white lines on the weight and dowel were measured with the aid of a travelling microscope. This procedure enabled the opening of the relay (and hence the application of the load on the fibre bundle) to be determined to within ± 1% of the duration of a test (typically 20 to 40 ms, being the time to either "steady state" deformation or failure of the bundle).

Once the timing of the test had been established it was possible, using a multiple linear regression program supplied by Mr. C.N. Anderson, to produce a polynomial equation describing the motion of the fibre bundle as a function of time. - This equation was differentiated to provide velocity and acceleration and hence the force on the fibre bundle was obtained. Further calculations, using simple bending theory provided value of Young's Modulus (E) and the extreme fibre stress (a) as functions of time. Figure A.3 is a plot of extreme fibre stress as a function of displacement for three of the fibre bundles which did not break under the loads indicated.

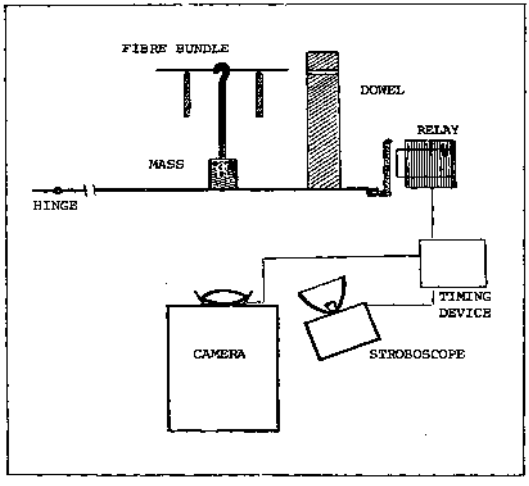

FIGURE A.l SCHEMATIC VIEW OF APPARATUS

FIGURE A.2 MULTIPLE EXPOSURES OF A FIBRE BUNDLE UNDER LOAD

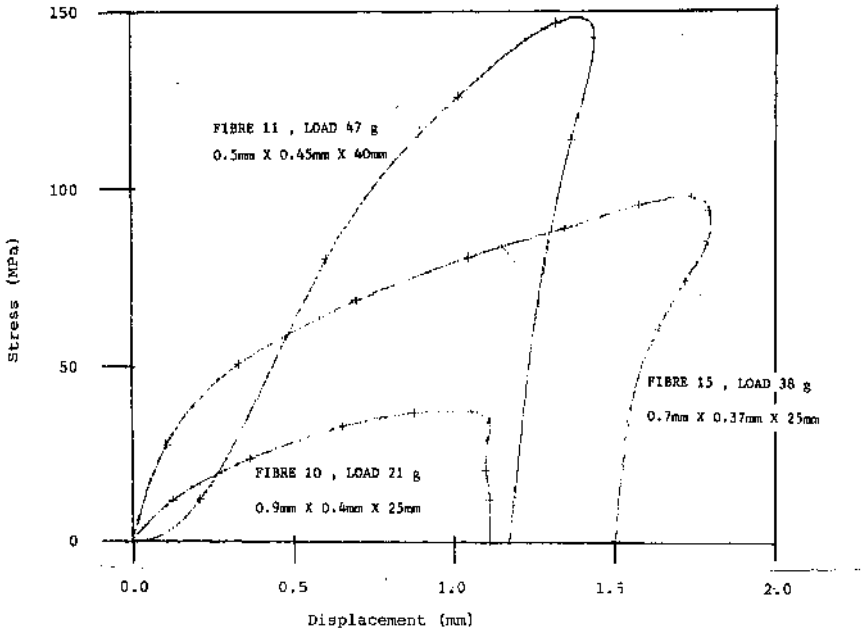

FIGURE A,3 RELATIONSHIP BETWEEN STRESS AND DISPLACEMENT FOR RAPID BENDING TESTS

APPENDIX B

PROBABILITY OF A MACROSTATE

In determining the number of microstates corresponding to a given macrostate, first take the molecular properties corresponding to the macrostate as given (i.e. take N values of the property A, of which N_1 are the value A_1, N_2 are the value A_2, etc....) and assess the number of ways the N beam elements can be assigned to these properties.

The first element may be allotted to one of N values

The second element may be allotted to one of (N-l) values

. . . . . etc.

whence the elements can be allotted to the N values in N! different ways.

However, taking this as the possible number of microstates would imply that the order in which the elements were arranged in each of the groups of identical values of A was important - i.e. for example, an element in the group corresponding to the value A_1 could take this value of A in N_1 different ways, and thus give rise to not one, but N_1 different microstates with no change in the distribution of the remaining molecules. This is incorrect, (since a given distribution of the values of A amongst the elements corresponds to a single microstate) whence, so far as this group is concerned, the number of possible microstates has been overestimated by a factor equal to the number of ways a given N_1 molecules can be rearranged within the group i.e. by a factor N_1 . A similar argument applies to the other groups, wherefore the number of possible microstates is correctly given by

$$\frac{N!}{N_1!\ N_2!\ N_3!\ \ldots\ldots\ldots}$$